



UNIVERSITY OF TRENTO

International PhD Program in Biomolecular Sciences

30th Cycle

“Beyond the Nuclear Pore Complex, Nup358 Clusters at the

Axon Initial Segment of Cultured Neurons”

Tutor

Prof. Paolo Macchi

CiBio

Ph.D. Thesis of

Bouchra Khalaf

CiBio

Academic Year 2016 - 2017

Declaration of Authorship

I declare that this thesis is a presentation of my original research work and has been composed entirely by myself, and that the use of all sources has been properly and fully acknowledged.

Bouchra Khalaf

ACKNOWLEDGEMENTS

This is it!! As a PhD student, I experienced all colors of emotions over the past four years but this thesis dissertation is quite the cherry on the cake and I wish to thank all the people who made this possible.

Firstly, I would like to express my gratitude to the University of Trento and the PhD school for granting me the scholarship to pursue my PhD degree. Thanks also go to my supervisor Prof. Paolo Macchi whose knowledge and expertise have guided me in my research path.

A special gratitude goes to Lorena Zubovic and Alessandro Roncador. I consider myself very fortunate to have you as lab mates and close friends. Thank you for always being there to help at both the professional and the personal levels. It was your encouragement and emotional support that I needed the most during this time. In brief, thank you for being my home away from home.

To all the sincere friends that I have in Cibio, thank you for being part of my experience and for bringing back the humor when I lost mine!

Finally, I would like to thank a special person in my life, my sister Iman. Even though we were distant, you have always been my comfort and inspiration. Thank you for your constant support and belief in my potentials. And to all my family, I say thank you. Without your love, I would not have finished this thesis.

ABSTRACT

Nup358 is the largest nucleoporin of around 358 kDa molecular weight that localizes on the cytoplasmic face of the nuclear pore complex (NPC). It takes part in the overall activity of the NPC mediating the transport of nucleic acids and proteins between the nucleus and the cytoplasm. However, due to its multi-domain configuration, Nup358 has a more pleiotropic function in several cellular mechanisms such as mediating the stability of microtubules and axon specification. Since little is known about the non-conventional role of Nup358 in neuronal polarity, my PhD thesis was focused on characterizing the subcellular distribution and expression pattern of Nup358 protein in cultured neurons. My results show Nup358 present at the nuclear rim of neuronal cells, associated with NPCs, also in the cytoplasm having a spotted pattern along the neuronal processes. Interestingly, Nup358 was remarkably clustered at the axon initial segment (AIS) of mature neurons and dependent on a prior recruitment of the master AIS scaffold, Ankyrin-G (AnkG), to this specific region. Of the distinct domains present in Nup358 protein, the N-terminal region was found to be crucial for its localization at the AIS. Further, changes in Nup358 protein expression were monitored during neuronal development. Indeed, I detected the presence of a shorter isoform of Nup358 that was increasing as neurons develop whereas the full-length protein had an opposite decreasing trend. To gain knowledge about the functional role of Nup358 in neurons, I investigated its protein expression/distribution in response to an increasing or decreasing neuronal activity with specific drug treatments. Surprisingly, Nup358 protein expression was reduced following the stimulation or the depolarization of neurons, mediated by calcium influx and NMDA receptors. Overall, my results show that Nup358 has a unique subcellular distribution in neurons, being enriched at the AIS at advanced stages of development, therefore, suggest an involvement of Nup358 protein in maintaining and modulating neuronal polarity and activity.

ABBREVIATIONS

4-AP	4-Aminopyridine	MAP2	Microtubule associated protein 2
5-EU	5-Ethynyl Uridine	MS	Mass spectrometry
ActD	Actinomycin D	MTs	Microtubules
AIS	Axon initial segment	MW	Molecular weight
AnkG	Ankyrin-G	NE	Nuclear envelope
AP	Action potential	Noc	Nocodazole
BIC	Bicuculline	NPC	Nuclear pore complex
CNS	Central nervous system	Nup	Nucleoporin
COX1	Cytochrome c oxidase 1	ONM	Outer nuclear membrane
CTX	cortex	RanBP2	Ran-binding protein
CY	Cyclophilin-like domain	RBD	Ran-GTP binding domain
Cyto D	Cytochalasin D	SpC	Spinal cord
DIV	Day <i>in vitro</i>	SUMO	Small ubiquitin-like modifier
DMSO	Dimethyl sulfoxide	TM Nups	Transmembrane Nups
Dvl	Dishevelled	TTX	Tetrodotoxin
EM	Electron micrograph		
ER	Endoplasmic reticulum		
FG-Nups	Phenylalanine-glycine Nups		
GFAP	Glial fibrillary acidic protein		
GFP	Green fluorescent protein		
HIPP	Hippocampus		
HKI	Hexokinase 1		
INM	Inner nuclear membrane		
IR	Internal repeats		
KBD	Kinesin binding domain		
LRR	Leucine-rich region		

Table of Contents

1. INTRODUCTION	1
1.1. An overview of the nuclear pore complex.....	1
1.2. The nucleoporins family	3
1.3. Dynamic Nups.....	6
1.4. Nup358	7
1.4.1. <i>Nup358 structure at a glance</i>	7
1.4.2. <i>Functional role in the nucleocytoplasmic transport</i>	8
1.4.3. <i>Implications in pathophysiology</i>	10
1.4.4. <i>Nup358 role beyond the NPC</i>	11
• In non-neuronal cells.....	11
• In neurons.....	12
1.5. The <i>in vitro</i> development of neurons	13
1.6. The Axon Initial Segment.....	14
2. AIM OF MY PHD PROJECT	16
3. RESULTS	17
3.1. Nup358 distribution pattern in mature cultured neurons	17
3.2. Among nucleoporins, Nup358 has a unique behavior in neurons.....	20
3.3. Nup358 subcellular distribution changes during neuronal development	22
3.4. Neurons express two isoforms of Nup358	25
3.5. Nup358 expression in different regions of the CNS	27
3.6. The N-terminal region is essential for Nup358 clustering at the AIS.....	30
3.7. Activity-dependent decrease in Nup358 protein expression	35
3.8. Neuronal depolarization with KCl reduces Nup358 expression through Calcium influx and NMDARs	39
3.9. Nup358 localization at the AIS does not depend on actin-microtubule cytoskeleton	43
3.10. AnkG is required for Nup358 localization at the AIS	46
4. DISCUSSION.....	48
4.1. Unique subcellular distribution of Nup358 in cultured cortical neurons	48
4.2. Two Nup358 isoforms.....	49
4.3. Nup358, a new player in the AIS architecture.....	51
4.4. Insight into the N-terminus domain of Nup358	53
5. OUTLOOK	54
6. MATERIALS AND METHODS	56
Bibliography.....	63

1. INTRODUCTION

1.1. An overview of the nuclear pore complex

The nuclear envelope (NE) is a double membrane that encloses the genetic material inside the nucleus and represents a physical barrier for contact with the cytoplasm. By this compartmentalization in eukaryotic cells, the NE not only separates the nucleus from the cytoplasm but also adds one level of regulation for gene expression, that is absent in prokaryotic cells. However, exchange of molecules between the nucleus and the cytoplasm is essential for maintaining cellular metabolism. Nuclear proteins such as DNA polymerases, RNA polymerases, RNA-processing proteins, transcription factors and histones, all are proteins crucial for the proper function of the nucleus yet are synthesized in the cytoplasm. In contrast, virtually all RNAs, including mRNAs, tRNAs, rRNAs, and miRNAs are synthesized in the nucleus and transported to the cytoplasm. These import/export pathways between the nucleus and the cytoplasm occur through pores of the NE, formed by the fusion of the outer and inner nuclear membranes (**Fig. 1-1**). As the number of pores present in the NE can vary between 3-5 NPC/ μm^2 ¹, a typical tissue cell can have roughly 2000–4000 pores in its NE². Occupying the space of these pores are large multiprotein complexes known as Nuclear Pore Complexes (NPCs) whose main role is to mediate the trafficking of protein and RNA between the nucleus and the cytoplasm^{3,4}.

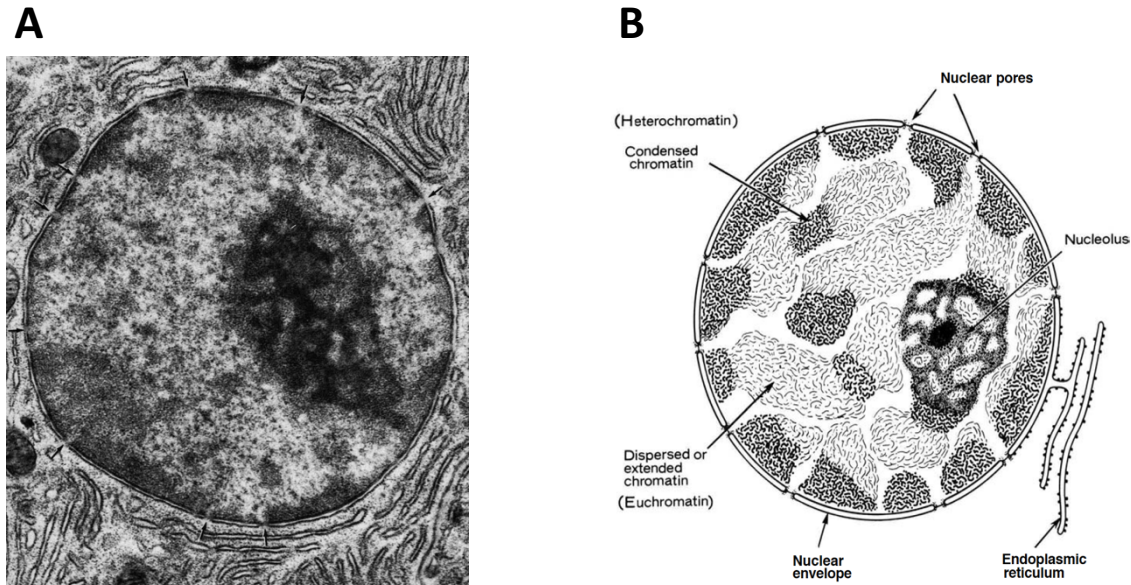


Figure 1-1 | A cross-section of a typical eukaryotic cell, with an emphasis on the structure of the nucleus. (A) An Electron Micrograph (EM) of a pancreatic acinar cell showing the nucleus surrounded by the nuclear envelope with the inner and outer nuclear membranes (INM and ONM) fused at certain intervals and thus forming nuclear pores that are marked by arrows. (B) Schematic drawing of the nucleus showing the major structural components: the condensed and the extended regions of the chromatin, namely the heterochromatin and the euchromatin respectively, the nucleolus which is the site of ribosome biogenesis, and the nuclear pores that traverse the NE, the latter of which is continuous with the endoplasmic reticulum (ER) studded with regularly spaced ribosomes (adapted from Fawcett et al., 1981⁵).

Nuclear pore complexes are the primary gateway for molecules to enter and exit the cell nucleus. Since their discovery in the 1950s, NPCs have been thoroughly studied to unravel their overall structure, molecular composition and function as transport channels between the nucleus and the cytoplasm. The NPC is considered one of the largest protein complexes in a cell, having a net molecular weight of 60 MDa in yeasts and approximately 120-125 MDa in vertebrate cells^{2,6-8}. Owing to its high molecular weight, the NPC structure of 120 nm diameter has been visualized using various techniques of electron microscopy. NPCs were thus described as channels traversing the NE, associated with 16 protein subunits, eight on the nucleoplasmic side and eight on the cytoplasmic side with radial symmetry across the nuclear envelope⁹. This octagonal structure of the NPC was inferred from electron micrographs of the nuclear and the cytoplasmic surfaces of the NE. However, a more detailed picture of NPCs structure and 3D-organization was only achieved through advancements in the fixation protocols and microscopy techniques such as field-emission in-lens electron microscopy, cryo-electron tomography, and single-particle reconstruction¹⁰⁻¹⁴. Altogether, studies of nearly 60

years of active research have delineated NPCs ultrastructure that comprises three distinct regions: the central transport channel with an embedded scaffold, and two rings located sideways, one cytoplasmic and the other nuclear, each is associated with eight filaments¹⁵. Whereas the cytoplasmic filaments are more flexible having their loose ends freely protruding towards the cytoplasm^{11,16}, the nuclear filaments are joined together in a distal ring forming a structure known as the nuclear basket (**Fig. 1-2**). This overall structure of NPCs is well-conserved from yeast to human even though there are considerable discrepancies in the protein composition, density and size of the NPC among species¹⁷⁻²⁰.

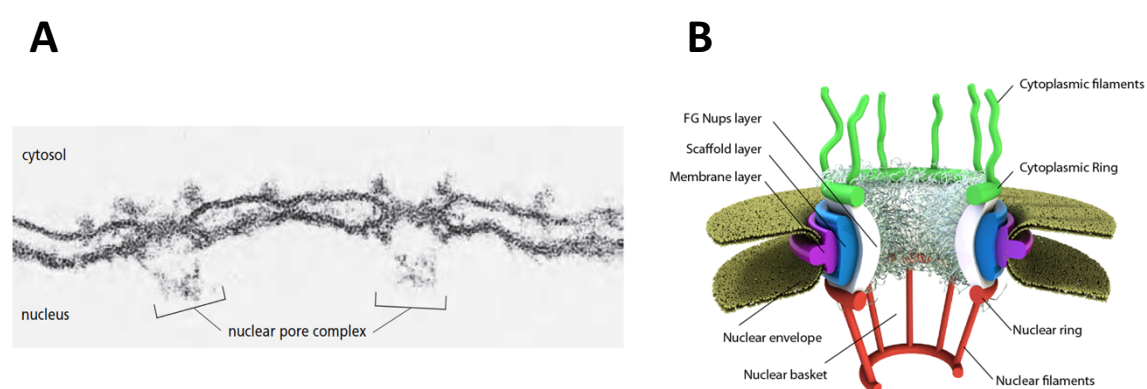


Figure 1-2 | The NPC architecture. (A) An EM of a cross-section view of an oocyte nucleus. In this view, two NPCs are identified spanning the NE²¹. (B) A schematic representation of the consensus model of vertebrate NPC²².

1.2. The nucleoporins family

Proteomic analyses of NPC protein composition revealed that despite its enormous size, the NPC is composed of only 30 different proteins termed as nucleoporins^{6,17,18,23}. Each nucleoporin is present in 8, 16, 32 or more copies per NPC, thus accounting for NPCs high molecular weight²⁴. Nomenclature of most nucleoporins is often denoted as Nup followed by a number corresponding to its molecular weight (MW), for instance, Nup107 in humans has a MW of 107 kDa whereas its homolog in yeast, Nup84 is of 84 kDa MW¹⁵.

Nucleoporins are arranged in biochemically defined subcomplexes, i.e. composed of stably interacting nucleoporins, which structurally represent the building blocks of the NPC¹⁸. In fact, the NPC is a modular assembly of a limited number of distinct subcomplexes²⁵. However, not all nucleoporins are identified within subcomplexes;

such nucleoporins might have a more dynamic characteristic or a relatively less stable interaction with one another than nucleoporins belonging to NPC subcomplexes. Therefore, nucleoporins are often grouped based on two factors, their association within subcomplexes and/or approximate localization in the overall structure of the NPC (**Fig. 1-3**): 1) the Y-complex, also known as coat nucleoporin complex (CNC), 2) adaptor protein complex present in the inner ring (known as Nup93/Nic96 complex), 3) central phenylalanine-glycine nucleoporins (FG-Nups), 4) transmembrane nucleoporins (TM Nups) or pore-membrane proteins (POMs), 5) nuclear-basket nucleoporins, and 7) a final category that includes a few unclassified nucleoporins²⁵⁻²⁷.

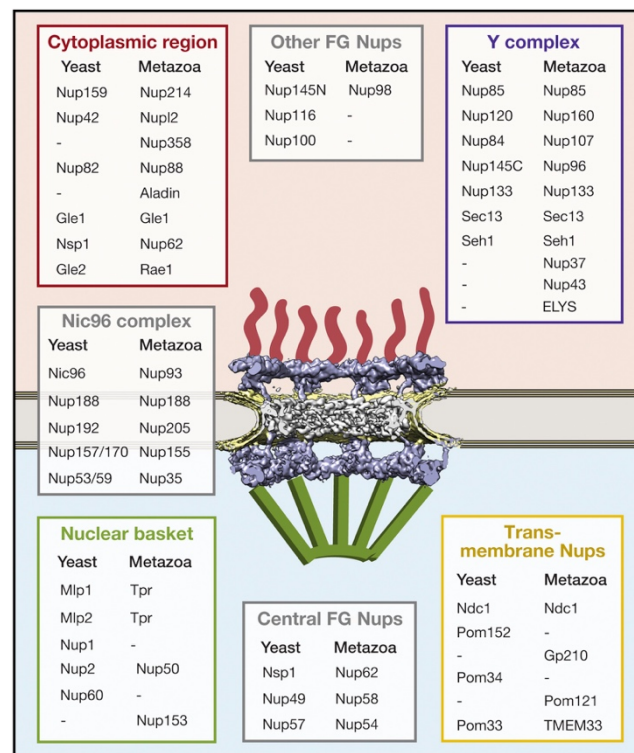


Figure 1-3 | Distribution of nucleoporins in the NPC overall structure. Side view of the NPC showing nucleoporins grouped according to their localization in the NPC and/or association within subcomplexes. Yeast nucleoporins and the corresponding metazoan variants are shown side to side with the (-) mark indicating that the homolog Nup is absent in the opposite species²⁸.

The Y-complex, known as Nup107-160 complex in humans, is considered the largest and best characterized NPC subcomplex. Depending on species, the Y-complex includes 6-10 Nups²⁹⁻³³. Nucleoporins of this subcomplex assemble in an elongated and branched structure similar in shape to the letter Y, hence its name the Y-complex³⁴⁻³⁶. It

is the scaffolding unit that represents the core of the NPC and gives the NPC its peculiar shape^{37,38}. Thus, Nups of this complex are located at the central channel and at both the nuclear and cytoplasmic rings^{36,39,40}.

The second main structural subcomplex is the Nup93/Nic96 complex that localizes at the inner ring of the NPC⁴¹⁻⁴⁴. In contrast to the Y-complex, the Nup93/Nic96 complex is less studied, though it describes a complex of five to seven nucleoporins including Nup93⁴¹⁻⁴³. The stoichiometry of nucleoporins within the Nup93/Nic96 subcomplex is not fully elucidated⁴⁵⁻⁴⁸, thus implying that the not all Nup93/Nic96 subcomplexes within the NPC are necessarily identical. However, Nup93 is particularly an indispensable nucleoporin depletion of which compromises the formation of both the NPC and the NE⁴⁹. Above all, localization of Nup93/Nic96 subcomplex en masse is essential to recruit and anchor Nup62 subcomplex to the NPC⁴³.

Lying in the center of the pore, Nup62 subcomplex establishes NPC's permeability barrier and represents a key element in the entire transport system across the pore⁵⁰. In eukaryotes, Nup62 subcomplex is formed of three nucleoporins belonging to the FG-Nups group⁴⁶. These Nups are characterized by the presence of up to 50 phenylalanine-glycine repeats (FG-repeats) distributed along their protein sequence^{51,52}. In structure, the FG-Nups of this trimeric Nup62 subcomplex assemble in disordered fiber-like extensions protruding from the central channel, thus forming the hydrogel meshwork that is a permeable yet a selective barrier for the transport of molecules across the NPC channel⁵³⁻⁵⁶.

Similar to the Y-complex, both the Nup93 and Nup62 subcomplexes serve a structural role in NPC's overall architecture. However, the NPC scaffold is anchored to the nuclear envelope by transmembrane Nups that, in metazoans, include the nucleoporins gp210, Ndc1, and POM121⁵⁷⁻⁵⁹. These TM nucleoporins, therefore, localize between the pore membrane and the central framework of the NPC.

To complete the NPC structure, the nucleoporins Nup153, Nup50 and Tpr assemble on the nucleoplasmic side in eight considerably long filaments, located ~100 nm from the plane of the NE, and joined together in the distal ring of the nuclear basket structure⁶⁰⁻⁶⁴. On the other side of the NPC, the nucleoporins Nup214 and Nup88 assemble in the so-called Nup214 subcomplex and, along with the nucleoporin Nup358,

build the cytoplasmic filaments that emanate from the NPC towards the cytoplasm^{65,66}. Compared to the nuclear filaments, cytoplasmic filaments are shorter, around ~35 nm, kinky and delicate filaments¹⁴.

1.3. Dynamic Nups

The NPC, as a whole entity, has a static nature, being stably embedded in the NE during the interphase period. During the cell cycle, the nucleus changes in shape, as a result, NPCs can move in arrays without having inherent mobility at the axial plane of the NE⁶⁷. Individual nucleoporins, instead, can be very dynamic in both dividing and non-dividing cells^{68,69}.

Even though nucleoporins comprise the NPC structure, many Nups can be found in the cytoplasm (or in the ER as for the transmembrane nucleoporin gp210), and/or the nucleoplasm⁶⁹⁻⁷². In a pilot study by Rabut et al. 2004, 19 out of the 30 nucleoporins were investigated for their dynamic characteristic. These 19 nucleoporins were tagged with green fluorescent protein (GFP), stably expressed in mammalian cells, and monitored for their dissociation rate from NPCs by inverse FRAP (iFRAP). iFRAP is a technique by which all fluorescent molecules in an entire cell are photobleached except for a small target region that is, in this case, the NPCs. The measurement of a nucleoporin dissociation rate from the NPC, or inversely its residence period at the NPC, was considered an indication of that nucleoporin dynamic ability. Results obtained were variable among the studied nucleoporins depending on two basic parameters: 1) the nucleoporin localization in the NPCs structure and 2) its functional role in NPCs overall activity. In brief, nucleoporins forming the core of NPCs were relatively more stable than peripheral nucleoporins that exhibited a more dynamic behavior. For example, nucleoporins belonging to Nup107-160 subcomplex had long residence period of more than 35 hours^{69,73} compared to Nup153 and Nup50 of the nuclear basket, that are highly dynamic with NPC residence periods in the minute range^{69,74}.

Indeed, this study concluded that nucleoporins can be classified based on their dynamic ability into three classes: scaffold, adaptor, and dynamic nucleoporins. Scaffold nucleoporins are stably associated with NPCs and have low dissociation rates while adaptor nucleoporins are relatively mobile with intermediate dissociation rates between

the scaffold and dynamic nucleoporins. Thus, the last class corresponding to dynamic nucleoporins is characterized by Nups of high dissociation rates; in other words, they are highly mobile compared to the rest of the studied nucleoporins⁶⁹. Whereas scaffolds serve a structural role in the NPC, dynamic nucleoporins such as Nup153 and Nup98 instead have a functional role in the nucleocytoplasmic transport, as they are essential for the export of RNA and import of nuclear proteins^{75,76}.

Up to now, little is known about the influence of nucleoporins dynamics in nucleocytoplasmic transport and cell physiology. However, a handful of reports have identified the involvement of specific nucleoporins in different cellular mechanisms such as cell migration, signaling, differentiation, regulation of genome architecture, and gene expression^{4,77-79}.

1.4. Nup358

Taking into consideration the reported dynamic feature of several nucleoporins, especially those located on the periphery of the NPC, Nup358 represents one good candidate worth an in-depth investigation for its dynamic behavior. Nup358 resides asymmetrically on the cytoplasmic filaments of the NPC structure⁸⁰. Though not classified within a specific NPC subcomplex, Nup358 interacts with the nucleoporins co-localizing at the cytoplasmic filaments, namely Nup214 and Nup88⁸¹. At the NPC, Nup358 has a pivotal role in the nucleocytoplasmic transport. However, a growing body of evidence identified non-conventional roles for this nucleoporin depending on its interaction with partner proteins.

1.4.1. Nup358 structure at a glance

Nup358 is a unique constituent of the metazoan NPC with no identified homolog in yeast. It was originally identified as a giant nuclear pore protein that binds to Ran⁸², a small GTP-binding nuclear protein, hence known also as Ran-binding protein 2 (RanBP2). This giant protein is by far the largest nucleoporin with an approximate molecular weight of 358 kDa^{82,83}. The human Nup358 protein sequence comprises 3,224 amino acid residues and includes a variety of functional domains (**Fig. 1-4**). Based on the motifs it harbors, Nup358 protein can be divided into several distinct regions: an N-terminal region of ~700-residues known as the leucine-rich region (LRR) containing a leucine

zipper motif, four homologous RanGTP-binding domains, eight tandem zinc finger motifs, a small ubiquitin-like modifier (SUMO) E3 ligase domain, and a C-terminal cyclophilin A homology domain⁸³. These domains are linked to each other by FG-repeats of the xFxFG pentapeptide sequence (where x represents any amino acid) distributed over the protein sequence and constitute the docking sites for transport receptors^{84,85}. While the different domains of Nup358 have been already identified, yet only the N-terminus, two Ran-binding domains, the SUMO E3 ligase domain, and the C-terminus have been structurally characterized^{86–90}. Despite that, the so-far structure-function studies on Nup358 have identified an increasing list of proteins to interact specifically with distinct domains of Nup358 protein sequence (see **Fig. 1-4**); thus, highlighting a rather intricate role of Nup358 in nucleocytoplasmic transport and the overall cellular activity.

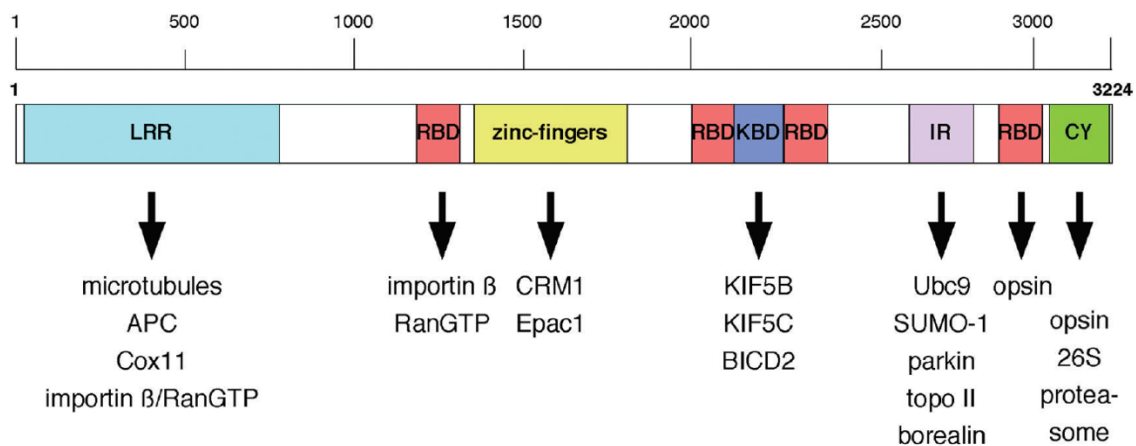


Figure 1-4 | Schematic representation of the human Nup358 protein. The 3,224-amino acid sequence comprises distinct domains and the corresponding interacting proteins. LRR, Leucine-rich region; RBD, Ran GTP-binding domain; zinc-fingers domain; KBD, kinesin-binding domain; IR, internal repeats; CY, cyclophilin A homology domain⁴.

1.4.2. Functional role in the nucleocytoplasmic transport

Around 1 million molecule/min crosses the NE of a metabolically active cell, mediated by the NPC. Restricted by their size, molecules can pass through the 9-nm diameter pore in a passive diffusion manner⁹¹. For instance, small sized molecules as cytochrome c (13 kDa) can easily cross the NPC, while ovalbumin (43 kDa) is slowly transported, and bovine serum albumin (66 kDa) is almost blocked from entering the pore⁹¹. On the other hand, macromolecules of diameter up to 25 nm are capable of

crossing the NPC through active transport controlled by the following main elements: energy consumption, signal dependence (nuclear localization signal; NLS and nuclear export signal; NES), transport receptors mostly karyopherins (importin and exportin), and saturability⁹¹⁻⁹³. The bidirectional flow of molecules across the NPC involves multiple proteins that are finely coordinated in elusive mechanisms.

In theory, Nup358/RanBP2 localization at the NPC periphery suggests its involvement in the transport of molecules into and out of the nucleus. Nup358 could interact with proteins to be imported to the nucleus and facilitate their entry, and oppositely Nup358 might contribute to the dissociation of cargo from the nucleus to the cytoplasm. In fact, several functional domains present in Nup358 protein proved to be binding sites for members of the nucleocytoplasmic transport machinery such as Ran^{83,86}. Ran participates in NPC transport mechanism via its GTPase cycle between GTP and GDP-bound states (**Fig. 1-5**). Relative to either state, Ran can differentially bind to specific proteins and consequently regulate the directionality of flow of molecules across the NPC⁹². In the import pathway, a specific importin binds to its designated cargo and facilitates its transport across the NPC. Once in the nucleus, RanGTP binds to the importin-cargo complex, mediates the release of the cargo and travels back to the cytoplasm associated with the importin receptor⁹⁴. In the export pathway, instead, exportin binds to both the cargo and RanGTP and all three in a complex pass through the NPC toward the cytoplasm⁹⁵. At the cytoplasmic face of the NPC, Nup358/RanBP2 contributes in the terminal step of the export of importin or exportin receptors to the cytoplasm. RanBP2 binds to RanGTP through the RBD and activates Ran GTPase-activating protein (RanGAP1) that indeed triggers GTP hydrolysis and subsequent disassembly of the complexes^{86,88,93,96,97}. Noteworthy that Nup358 is not only capable of binding Ran protein but, as it has been reported previously, Nup358 protein harbors docking sites for binding the heterodimeric mRNA export receptor, NXF1-p15, and the export factor, exportin-1^{98,99}.

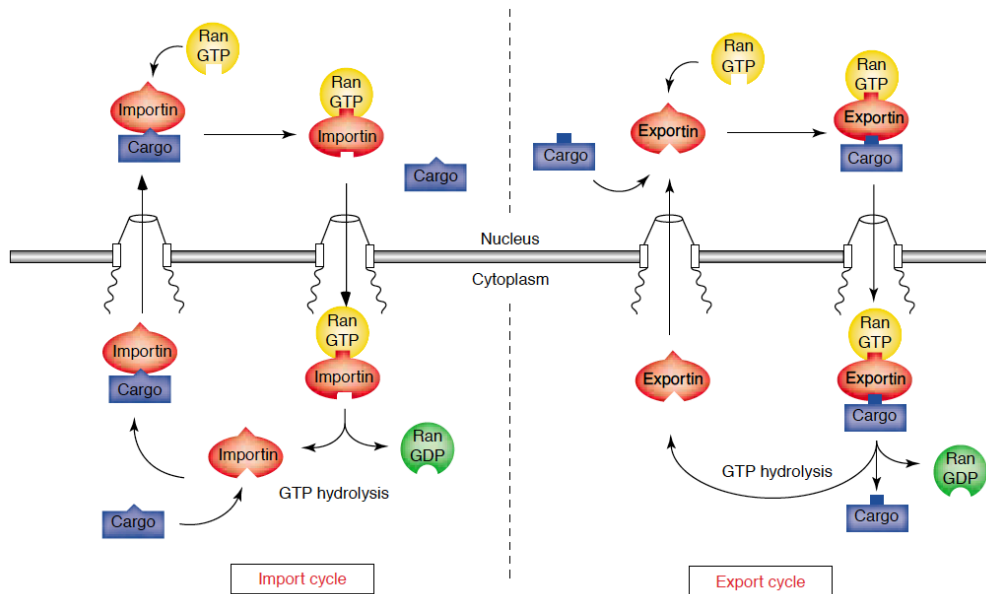


Figure 1-5 | The Ran-GTPase cycle during the import/export pathways. During the import cycle (left), importin binds to its cargo in the cytoplasm then is transported into the nucleus through the NPC. In the nucleus, RanGTP binds to importin and the cargo is released. The importin/RanGTP is then recycled into the cytoplasm, where RanGTP dissociates from the importin, and GTP is hydrolyzed into GDP by the action of the Ran-GTPase. While in the export cycle (right), RanGTP binding to exportin in the nucleus induces binding to the cargo and its transport through the NPC to the cytoplasm, where GTP hydrolysis takes place and thus the cargo is free in the cytoplasm and the exportin is recycled back to the nucleus¹⁰⁰. In either pathway, the GTP hydrolysis is induced by RanBP2 binding to RanGTP, following which RanGTPase 1 is activated.

1.4.3. Implications in pathophysiology

In humans, a few missense mutations in *RanBP2* gene, specifically in the leucine-rich region, have been linked to the susceptibility of familial and recurrent acute necrotizing encephalopathy (ANE)¹⁰¹. ANE is a rapid and progressive encephalopathy that occurs to previously healthy children following their encounter of viral infections as mycoplasma, influenza and herpes simplex virus. Though there is no strong link between Nup358 malfunction and a specific syndrome or disease, several studies were performed on mouse models to identify the involvement of Nup358 in pathophysiology. *Nup358/RanBP2*^{-/-} mice are embryonic lethal, while the haploinsufficiency of *RanBP2* causes the levels of the enzyme hexokinase-1 (HK1) and ATP to drop down selectively in the central nervous system. Whereas non-neuronal cells maintain normal levels of HK1 and ATP; this suggests a link between Nup358 and neuronal metabolism¹⁰². Further, a recent study showed that conditional ablation of Nup358 in mouse motoneurons resulted in various traits that resembled ALS-like syndrome such as hypoactivity,

hindlimb paralysis, and decreased nerve conduction velocity. These defects were primarily related to disruptions in the nucleocytoplasmic partitioning of importin- β and exportin-1 and in chemokine and metalloproteinase signaling¹⁰³.

Alternative studies done on mammalian cell lines demonstrated that Nup358 loss has no significant consequence on protein import into the nucleus but slightly affects the export of mRNA and signal-bearing proteins⁸¹. In neuronal cell lines, Nup358 was shown to be a substrate for Parkin, one causative agent of autosomal recessive juvenile parkinsonism (AR-JP). Upon binding to Parkin, Nup358 is ubiquitinated and degraded via the proteasome pathway, thus implying Nup358 involvement in the pathogenesis of Parkinson's disease¹⁰⁴. Moreover, a recent report indicates that Nup358 binds through its RBD3 to ubiquitin and regulates its levels in neurons in an age-dependent manner¹⁰⁵.

1.4.4. Nup358 role beyond the NPC

Due to its multi-domain configuration, Nup358 role is not only limited to facilitating nucleocytoplasmic transport but, Nup358 has a more pleiotropic function in the regulation of several cellular activities.

- In non-neuronal cells

Cell division in eukaryotic cells includes several distinct steps, where NPCs disassembly and assembly cycle is fundamental in such ordered process. Early following the nuclear envelope breakdown, NPCs disassemble in a synchronous yet fast manner. Fragments of the NE and the transmembrane nucleoporins retract to the ER whereas soluble nucleoporins disperse in the cytoplasm as stable subcomplexes⁴⁴. Some of these nucleoporins take part in the mitotic spindle apparatus comprising the kinetochores, centrosome and spindles^{44,106}. Nup358, associated with RanGAP1, relocates to microtubules (MTs) and mediates their stability. By attachment to MTs, Nup358 modulates microtubule–kinetochore interactions and regulates the association of other components with the kinetochores^{107,108}. Additionally, Nup358 role extends to later phases in the mitotic process. After chromosomes are correctly positioned on microtubules and prior to anaphase, Nup358 sumoylates Topoisomerase II α enzyme that in turn acts on decatenation of sister chromatids off the centromeres¹⁰⁹. Thus, Nup358 involvement is crucial throughout the mitotic process, without which the cells would

enter into mitotic arrest at the G2/M phase, experience abnormal chromosome segregation, metaphase catastrophe, and formation of anaphase bridges^{109,110}.

Moreover, during the interphase period of mammalian cell lines, Nup358 was found to be associated as well with microtubules. While the bulk of Nup358 is incorporated with NPCs at the nuclear rim, a fraction of the total pool of Nup358 localizes in the cytoplasm at the tips of cell extensions. This cytoplasmic fraction of Nup358 binds to and promotes the stability interphase microtubules¹¹¹.

Besides that, a few studies have shown that Nup358 is involved in the regulation of mRNA translation through different mechanisms. On the one hand, Nup358 interacts with specific mRNAs encoding secretory proteins and potentiates their translation¹¹². And on the other hand, Nup358 contributes in translational repression of target mRNA through binding to RNA and protein components of the miRNA-induced silencing complex (miRISC)¹¹³.

- In neurons

A former study led by Paulo Ferreira aimed to examine whether Nup358 has a ubiquitous or a cell (tissue)-specific expression profile. *Nup358* gene expression analysis was conducted on various tissues including the liver, spleen, lungs, kidneys, skeletal muscle, retina, heart and brain; whereby *Nup358* was found to be highly expressed in the retinal tissue¹¹⁴. Relative to differences among cell subtypes of the neuroretina, photoreceptors and some ganglion cells exhibit a relatively high expression level of Nup358 and a distinctive distribution pattern¹¹⁵. In these cells, Nup358 is not only present associated with the NPC, but also in the cytoplasm in the form of discrete spots spatially located away from the nuclear rim. Distinct domains of Nup358 were found to interact selectively with retina-specific proteins and consequently influence the neuronal function. The RBD4 and CY domains of Nup358 act as selective chaperones for red/green opsins in cone photoreceptors^{116,117}. Another functional motif of Nup358, located between RBD2 & RBD3, associates with the neuronal KIF5C and the ubiquitous KIF5B microtubule-dependent motor proteins in a subpopulation of neuronal cells^{118,119}. Additionally, the CY domain can associate with certain subunits of the 19S cap of

the 26S proteasome pathway ¹²⁰, therefore suggesting that Nup358 might be a key element for integrating the proteasome pathway with protein biogenesis ¹²⁰.

Further, Nup358 localizes in the mitochondria-rich ellipsoid compartment of cone and rod photoreceptors ¹¹⁵, and particularly associates through its LRR with the mitochondrial metallochaperone Cox11, and the central enzyme in glycolysis, HKI ¹⁰². This distribution pattern of Nup358 can be observed in different regions of the central nervous system (CNS) ¹⁰². In the same neuronal context, Nup358 interacts through its N-terminus with members of the Par polarity complex, such as Dishevelled (Dvl) and atypical protein kinase (aPKC), to modulate neuronal polarity and axon specification in cultured hippocampal neurons ¹²¹. All in all, the multi-functional role of Nup358 varies according to its interaction with partner proteins in a cell-type dependent fashion. Considering the previously mentioned studies, Nup358 might be specifically correlated with the overall activity of neurons and possibly be implicated in neurological diseases.

1.5. The *in vitro* development of neurons

Neurons are amazingly polarized cells with two distinct compartments: the somatodendritic and axonal compartments. These two domains differ in not only their morphological characteristics but also in their molecular composition and function. Based on dendritic/axonal polarity, neurons can receive, integrate and transmit an electrochemical signal throughout the nervous system; thus, maintaining polarity is essential for proper neuronal function. Over the past decades, cultured hippocampal pyramidal neurons have been used as a model system to study the stages of axon-dendrite differentiation during the *in vitro* neuronal development ¹²². To obtain their characteristic morphology, cultured neurons pass through five main stages (**Fig. 1-6**). Early after plating, i.e. during the first 24 hr in culture, neurons undergo a fundamental transition in their shape exhibited by the rapid outgrowth of one neurite over the rest. This neurite differentiates to become the axon whereas the remaining neurites develop into the dendrites. Based on this model of *in vitro* cultured neurons, axon specification represents the initial and central event that breaks the symmetry and gives the neuron its typical polarized morphology.

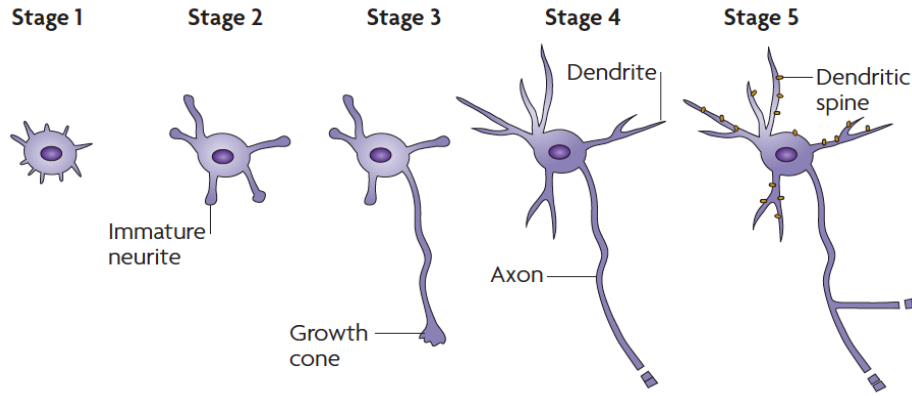


Figure 1-6 |Sequential events of establishing neuronal polarity in cultured hippocampal neurons. A schematic drawing of cultured hippocampal neurons showing the five main stages during which neurons acquire their characteristic morphology. Shortly after plating, neurons appear round with few protrusions (Stage 1). These minor processes, actively extending and retracting, develop into immature neurites of an almost identical length (Stage 2). Of these neurites, one starts to grow at a higher rate and transforms into the axon thus breaking the symmetry of neuronal cells (Stage 3). The axon continues to grow in the following days and the remaining neurites differentiate into dendrites, which are relatively shorter processes with tapering ends (Stage 4). The final stage involves dendritic arborization, formation of synaptic contacts and establishment of the neuronal network (Stage 5)¹²⁴.

1.6. The Axon Initial Segment

Though changes in morphology might be easy to monitor, the establishment and maintenance of neuronal polarity require a complex yet concerted involvement of intracellular/extracellular mechanisms and cytoskeletal dynamics¹²³. In the first days in culture and after axon specification, a unique highly-specialized region called the Axon Initial Segment (AIS) is identified within the first 50- μm of the proximal part of the axon in most neurons. The AIS is formed during the transition from stage 3-4 (see **Fig. 1-6**) which is around three to four days of the *in vitro* development of hippocampal neurons¹²⁵. Besides its role in maintaining neuronal polarity, the AIS has a diffusion barrier and intracellular sorting system that selectively restrict the trafficking of proteins to either the axonal or somatodendritic domains¹²⁶. Thus, the AIS represents a physical and physiological barrier between the somatodendritic and axonal domains^{127,128}. Interestingly, the AIS is the site responsible for the generation action potential (AP) due to the high density of ion channels present at this specific domain of a neuron¹²⁹. The protein composition of the AIS includes, as well, a few extracellular matrix molecules, cell-adhesion molecules, and cytoskeletal scaffold proteins (**Fig. 1-7**). Of

these proteins, a giant protein, known as Ankyrin-G (AnkG), acts as the master AIS scaffold that orchestrates the assembly and the clustering of other AIS proteins ¹²⁷.

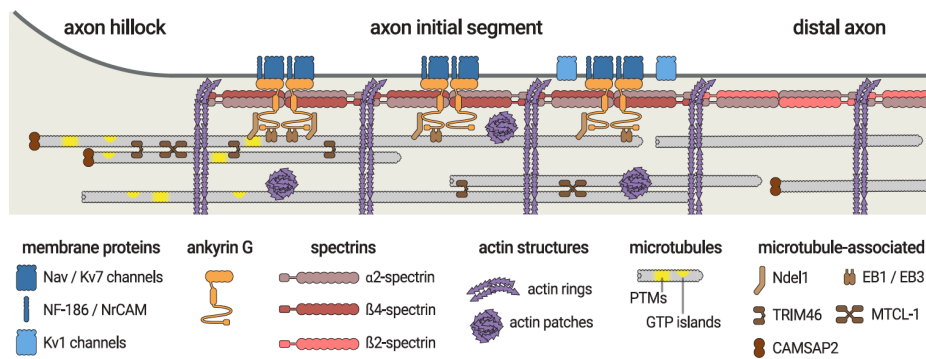


Figure 1-7 | The Axon Initial Segment Protein Composition. A schematic drawing of the AIS architecture. The AIS of neurons is composed of a high density of the ion channels, Na_v and K_v, that are shown bound to Ankyrin-G. AnkG binds α2 and β4-spectrin and associates with microtubules via EB1/EB3 and Ndel1, in the sub-membranous area. Actin is shown as periodic rings along the AIS ¹³⁰.

While the protein composition of the AIS has already been characterized, the mechanisms that control the targeting of AIS proteins to their ultimate destination remain poorly understood. Nonetheless, as neuronal plasticity has been a hot topic for investigation, AIS plasticity has also been reported recently. A few studies in the field have shown that the AIS architecture can be modulated by the developmental stage of the neuron or by altered neuronal activity. For instance, an increased neuronal activity would allow calcium influx through NMDA or P2X receptors consequently, Nav and Kv channels are endocytosed from the AIS plasma membrane ¹³⁰. Moreover, changes in neuronal activity could also modulate the morphology of the AIS; an increased activity results in a shift of the AIS toward the distal region of the axon whereas a decreased activity is often linked to an increased length of the AIS ¹³⁰.

Indeed, the AIS is a compartment essential for neuronal excitability and polarity. Though a great deal of knowledge is achieved about its role and protein composition yet the AIS modulation and correlation with neurological diseases are not fully elucidated.

2. AIM OF MY PHD PROJECT

Nuclear pore complexes are multiprotein complexes embedded in the nuclear envelope of eukaryotic cells and best known for their central role in mediating nucleocytoplasmic trafficking. However, this view of NPCs static nature and function has evolved over the past decade. NPCs, or more accurately its constituting proteins have a rather dynamic characteristic that renders them capable of dissociating off the NPC and taking part in the regulation of cellular activities in a cell type-specific fashion.

Nup358 is one constituent of the NPC that has a dynamic characteristic in a cell-type dependent manner. Based on previous studies, Nup358 was found to be involved in axon specification by interacting with the Par polarity complex; without Nup358, cultured neurons would develop multiple axons instead of an only one axon. Besides that, the multi-domain configuration of Nup358 promotes selective interaction with specific proteins in certain subtypes of the neuron; consequently, Nup358 acts as a chaperone for these proteins to reach their destination in the neuronal cell.

To this end, I assume that Nup358 might have a central role in the establishment or the maintenance of polarity in cultured neurons.

To address this topic, I outlined three broad objectives:

- Investigate the subcellular distribution pattern and protein expression of Nup358
- Examine changes in Nup358 behavior during the in vitro development of neurons
- Test the effect of various pharmacological treatments on Nup358 profile and expression to investigate possible correlation between Nup358 behavior and neuronal activity

3. RESULTS

3.1. Nup358 distribution pattern in mature cultured neurons

Apart from its classical association with NPCs and involvement in the nucleocytoplasmic transport, previous reports have shown that Nup358 is capable of binding and modulating the stability of microtubules in mammalian cell lines^{107,111}. Microtubules (MTs), in neuronal cells, have a central role in numerous cellular and developmental processes including neuronal polarity, differentiation and intracellular trafficking¹³³. Thus, I aimed to analyze the subcellular localization of Nup358 relative to MTs as a first step toward characterizing Nup358 protein in cultured neurons. 14 days *in vitro* (DIV) mouse cortical neurons were immunostained for Nup358 and β III-tubulin, a neuron-specific marker for microtubules. As expected, Nup358 decorated the boundaries of cell nuclei due to its association with NPCs at the nuclear envelope (**Fig. 3-1, A**). However, Nup358 was expressed as well in the cell soma and the neuronal network, and remarkably enriched in specific processes originating from individual neuronal cells (**Fig. 3-1, A; Arrowheads**). To identify the nature of these processes, whether dendritic or axonal, cultured neurons were immunostained for the dendritic marker MAP2. Consequently, Nup358 was shown clustered in the processes where MAP2 signal was excluded (**Fig.3-1, B**), thus suggesting that Nup358 localizes, preferentially, in the axon or more specifically in the axon initial segment (AIS) as the high-intensity signal of Nup358 was restricted to the first part of the MAP2-free processes. Indeed, co-immunostaining for the AIS marker, Ankyrin-G (AnkG), showed an almost perfect overlapping with Nup358 fluorescence signal at the AIS (**Fig. 3-1, C**).

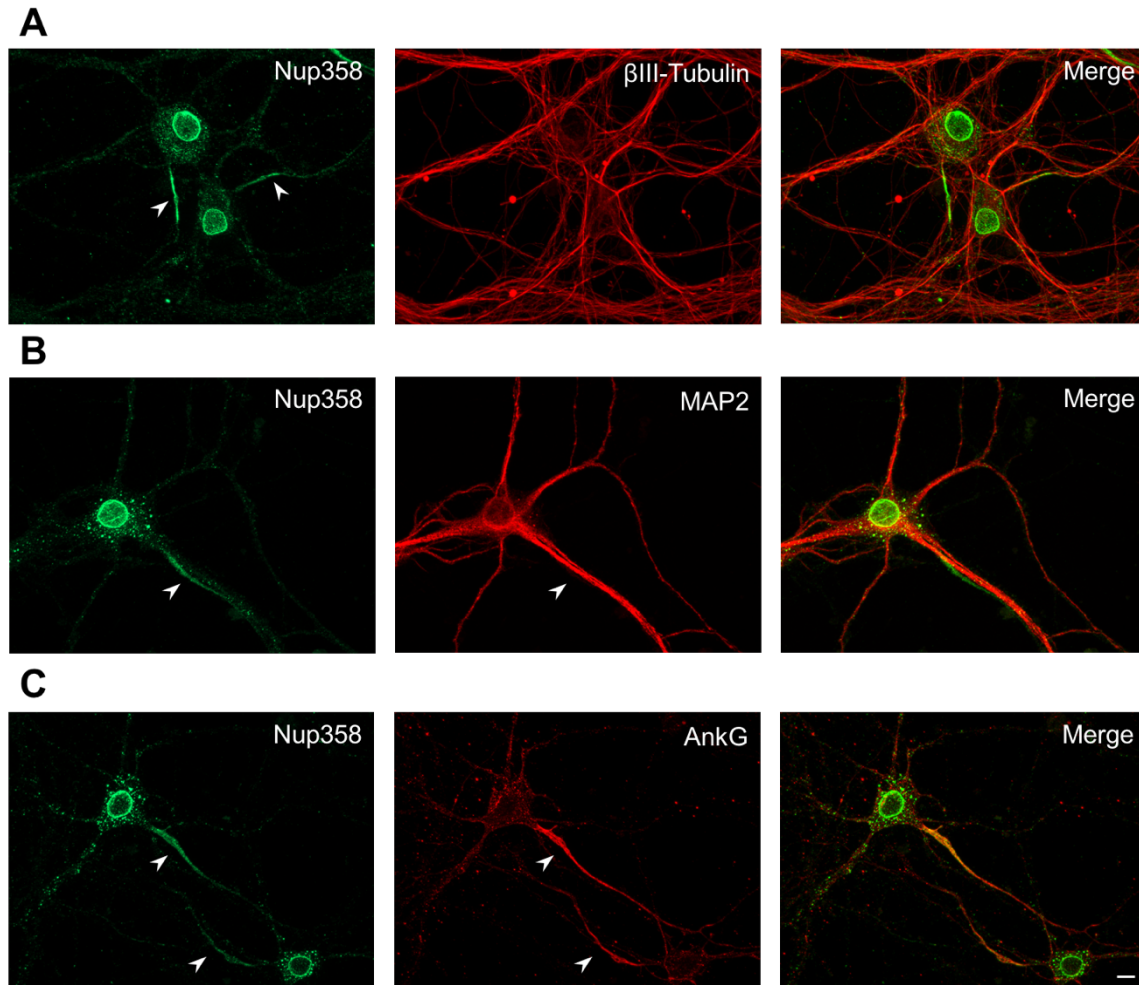


Figure 3-1 | Nup358 clusters at the axon initial segment of mature cortical neurons. 14 DIV mouse cortical neurons were co-immunostained for Nup358 (green) and: (A) β III-tubulin, a microtubule marker, (B) MAP2, microtubule-associated protein 2 present exclusively in dendrites, and (C) AnkG, a scaffold protein present in high density at the axon initial segment (red). Arrowheads mark the high fluorescence intensity of Nup358 in specific regions of the neuronal network identified by the lack of MAP2 signal in (B) or by the overlapping with AnkG staining in (C). (Scale bar: 10 μ m).

Because one fraction of the total pool of Nup358 had a spotted pattern in the cell body of neurons, I assessed whether these Nup358 puncta lie within any of the major subcellular compartments and organelles: the endoplasmic reticulum (ER), the Golgi apparatus and the mitochondria. Accordingly, cortical neurons were co-immunostained for the following markers: Calnexin for detecting the ER (**Fig. 3-2, A**), p58 as a *cis*-Golgi marker (**Fig. 3-2, B**), and COX1 as a marker for mitochondria (**Fig. 3-2, C**). In contrast to some previous studies where Nup358 was identified in the mitochondria of neuronal cells^{102,115}, our cultures of mouse cortical neurons show Nup358 discrete puncta mainly present in the ER whereas in juxtaposition with the Golgi and absent from the

mitochondria. Such differences in the subcellular distribution of Nup358 could, however, be influenced by differences among cell types.

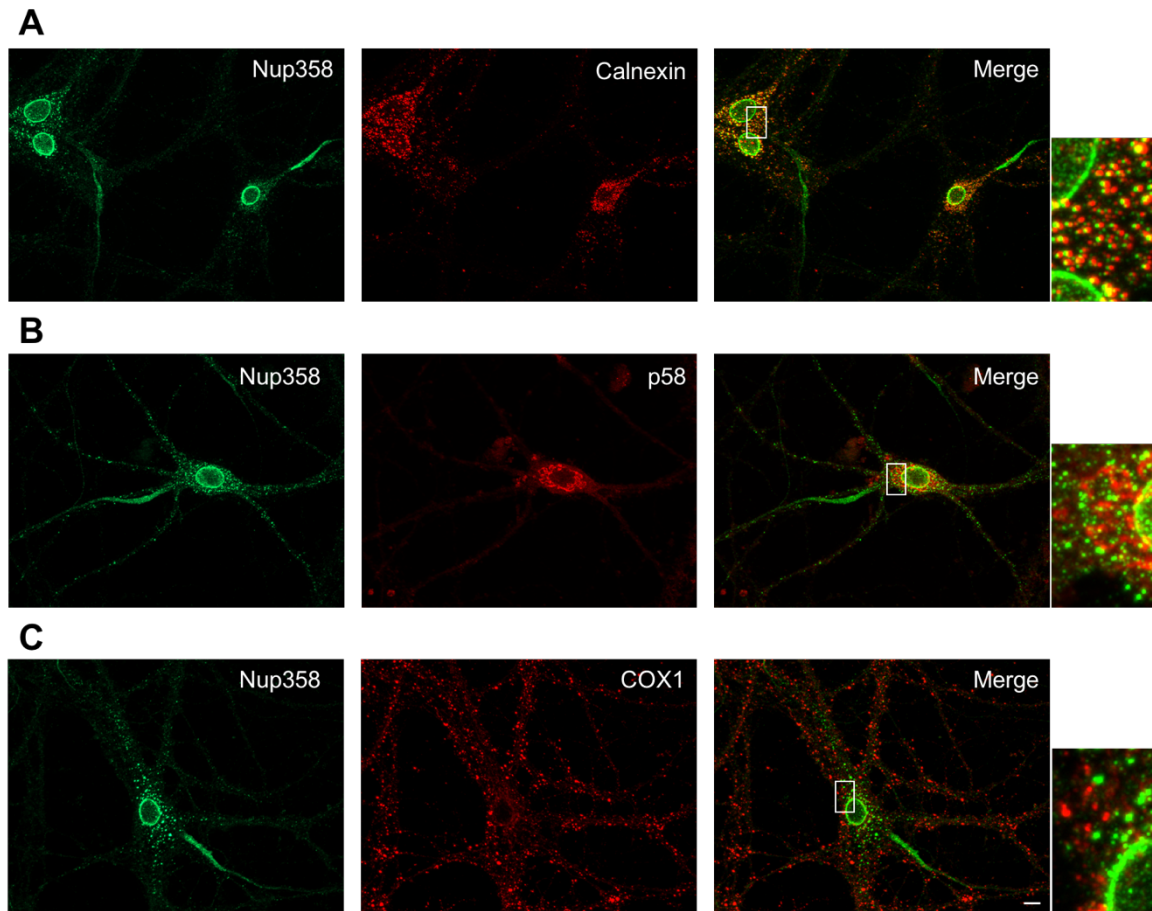


Figure 3-2 | Nup358 somatodendritic puncta co-localize with the endoplasmic reticulum. Immunostaining of mature 14 DIV cortical neurons for Nup358 and markers of the main cellular organelles: (A) Calnexin as a marker for the endoplasmic reticulum, (B) p58 for the Golgi apparatus, and (C) cytochrome c oxidase I (COX1) for the mitochondria. Note that Nup358 punctate pattern in the cell soma overlaps only with the endoplasmic reticulum staining, as depicted in the magnified views of the boxed areas, shown on the right of the overlay images. (Scale bar: 10 μ m).

Taken together, these results demonstrate that Nup358 subcellular localization is not restricted by its association with NPCs at the nuclear envelope. Instead, Nup358 has a more dynamic behavior, present in a punctate pattern in the cell soma and neuronal processes, and clustered at the AIS of mature neurons. As the AIS is a unique neuronal compartment, in both its physiological function and physical architecture, this finding underlies an unprecedented involvement for a nucleoporin, Nup358, in the overall function of neurons.

3.2. Among nucleoporins, Nup358 has a unique behavior in neurons

The intracellular expression of Nup358 in areas other than the NE reflects its dynamic behavior in neuronal cells. However, a few other nucleoporins were reported to have a dynamic behavior as well, according to their position in the NPC architecture and their functional role in nucleocytoplasmic trafficking⁶⁹. Thus, to better identify whether nucleoporins are commonly present in the cytoplasm of neuronal cells or that this is a unique feature of Nup358, 14 DIV cortical neurons were immunostained using Nup358 antibody and a generic anti-nuclear pore complex proteins, antibody m414 (**Fig. 3-3, A**). In parallel, immunostaining was conducted against Nup358 and the following specific nucleoporins: Nup153 of the nuclear basket structure (**Fig. 3-3, B**), Nup98 that resides on both the nuclear and the cytoplasmic rings of the NPC (**Fig. 3-3, C**), and most importantly Nup88 that associates with and anchors Nup358 at the cytoplasmic filaments of the NPC (**Fig. 3-3, D**). Apart from Nup358, all the tested nucleoporins were expressed at the NE due to their association with the NPCs. These nucleoporins exhibited a sharp perinuclear staining whereas no signal was detected in either the cell soma or neuronal processes. Nup358, alternatively, had a unique distribution pattern in neurons, that extends beyond the perinuclear region and does not necessarily depend on its interaction with the nucleoporin Nup88.

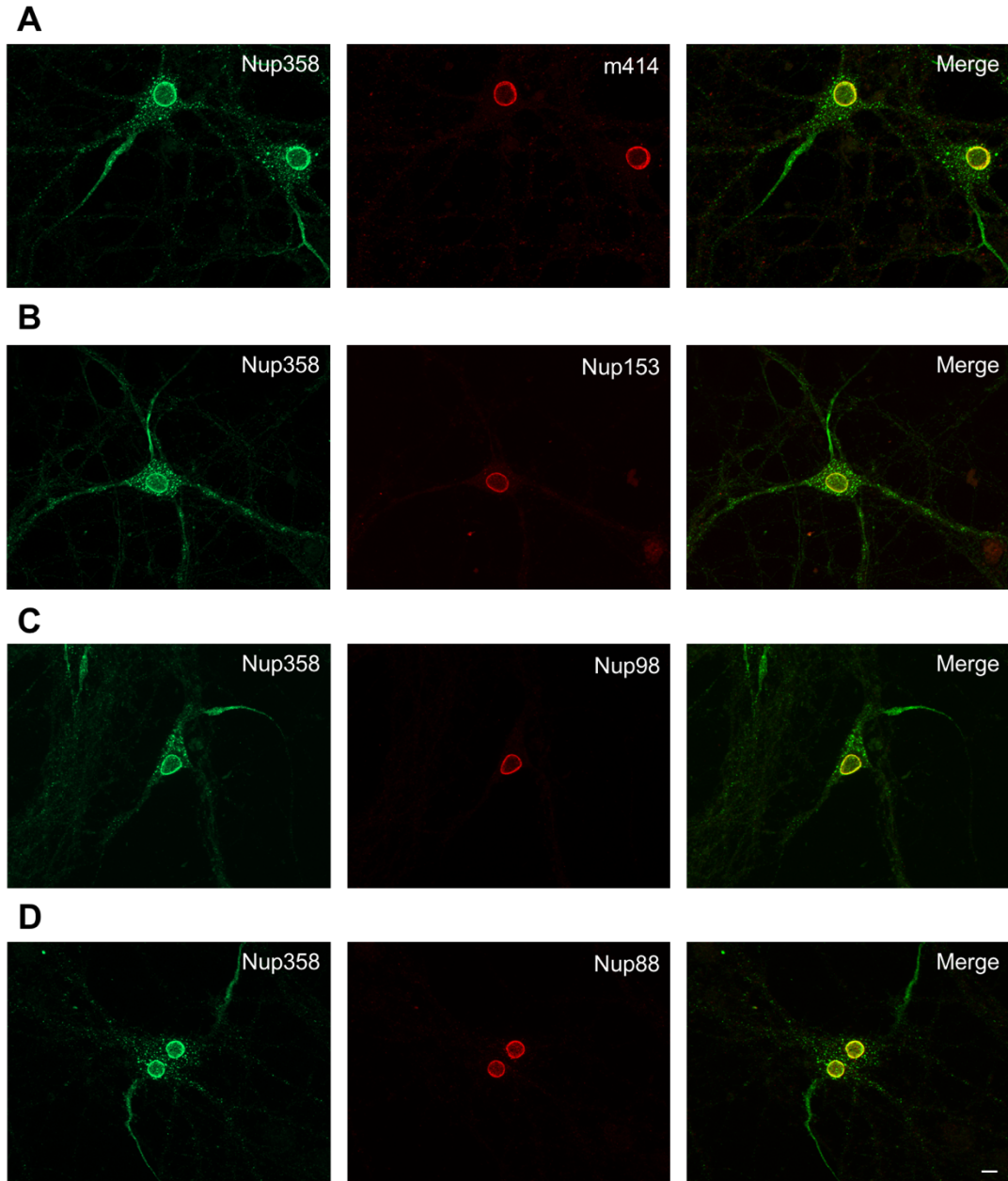


Figure 3-3 | The subcellular distribution of Nup358 relative to other nucleoporins of the NPC. (A) Mature 14 DIV mouse cortical neurons were immunostained using an antibody against Nup358 and the antibody m414 that recognizes multiple nucleoporins having phenylalanine-glycine repeats (FG). (B-D) Alternatively, 14 DIV cortical neurons were co-immunostained for Nup358 and: (B) Nup153 of the nuclear basket structure, (C) Nup98 present at both faces of the NPC, or (D) Nup88 present at the cytoplasmic filaments of the NPC. Apart from Nup358, nucleoporins are preferentially expressed at the perinuclear region demonstrated by a crisp ring around cell nuclei, with a minimal or absent signal in the cytoplasm. (Scale bar: 10 μ m).

Since the NPC mediates nucleocytoplasmic transport of molecules including RNAs, several nucleoporins such as Nup98 and Nup153 are known to interact with transcribed RNAs and assist their export to the cytoplasm. In this context, the mobility of these Nups on/off the NPC is transcription-dependent⁷⁶. To investigate whether the

subcellular distribution of Nup35 is influenced by RNA transcription, 14 DIV cortical neurons were treated with Actinomycin D (ActD; 5 $\mu\text{g}/\text{ml}$, 1 hr) to inhibit transcription by both RNA polymerases I and II. And to verify the efficiency of the ActD treatment, neurons were co-treated with 5-EU, a Uracil analog, that gets incorporated into nascent RNAs during active transcription and can be detected with a click reaction using the fluorescent dye, 5-FAM (details are in the Materials & Methods section). While control neurons showed 5-EU labeling of newly synthesized RNAs in cell nuclei, ActD-treated neurons had no detectable signal for an active transcription. However, with respect to Nup358 distribution pattern, no change was observed regardless of whether the ActD treatment was included or not, thus ruling out the role of RNA transcription in the subcellular distribution profile of Nup358 (Fig. 3-4).

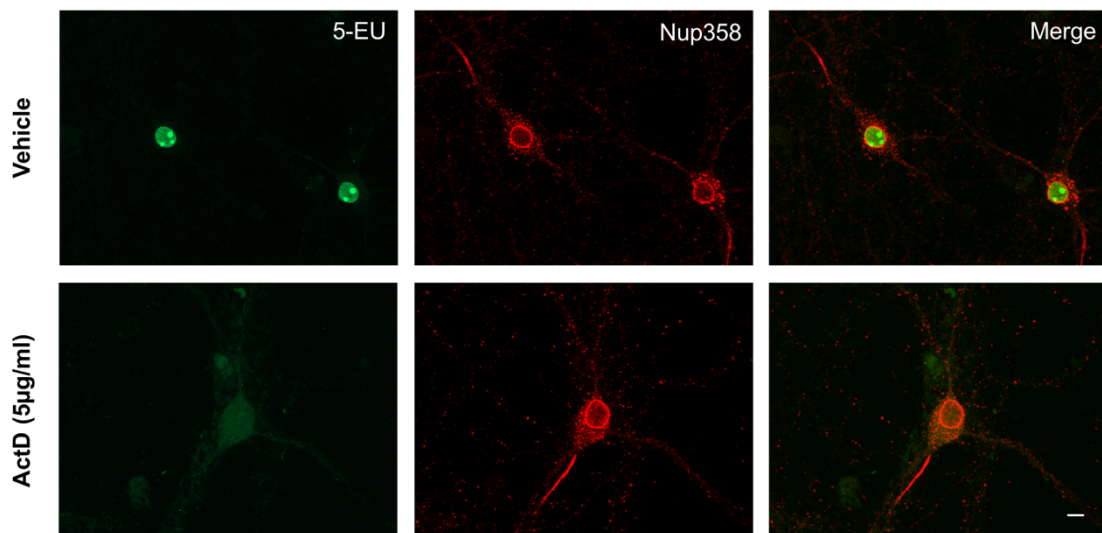


Figure 3-4 | Nup358 distribution pattern is not sensitive to the inhibition of RNA transcription. Cultured neurons were treated with DMSO as control (vehicle), or ActD (5 $\mu\text{g}/\text{ml}$; 1 hr) to inhibit RNA polymerases I and II. In both conditions, neurons were simultaneously incubated with 5-EU, an artificial analog for Uracil that gets incorporated in RNA during active transcription. As a result, 5-EU was present in the nuclei of control neurons whereas absent in ActD-treated cells. Immunostaining for Nup358 showed similar distribution patterns of Nup358 in both treated and untreated neurons. (Scale bar: 10 μm).

3.3. Nup358 subcellular distribution changes during neuronal development

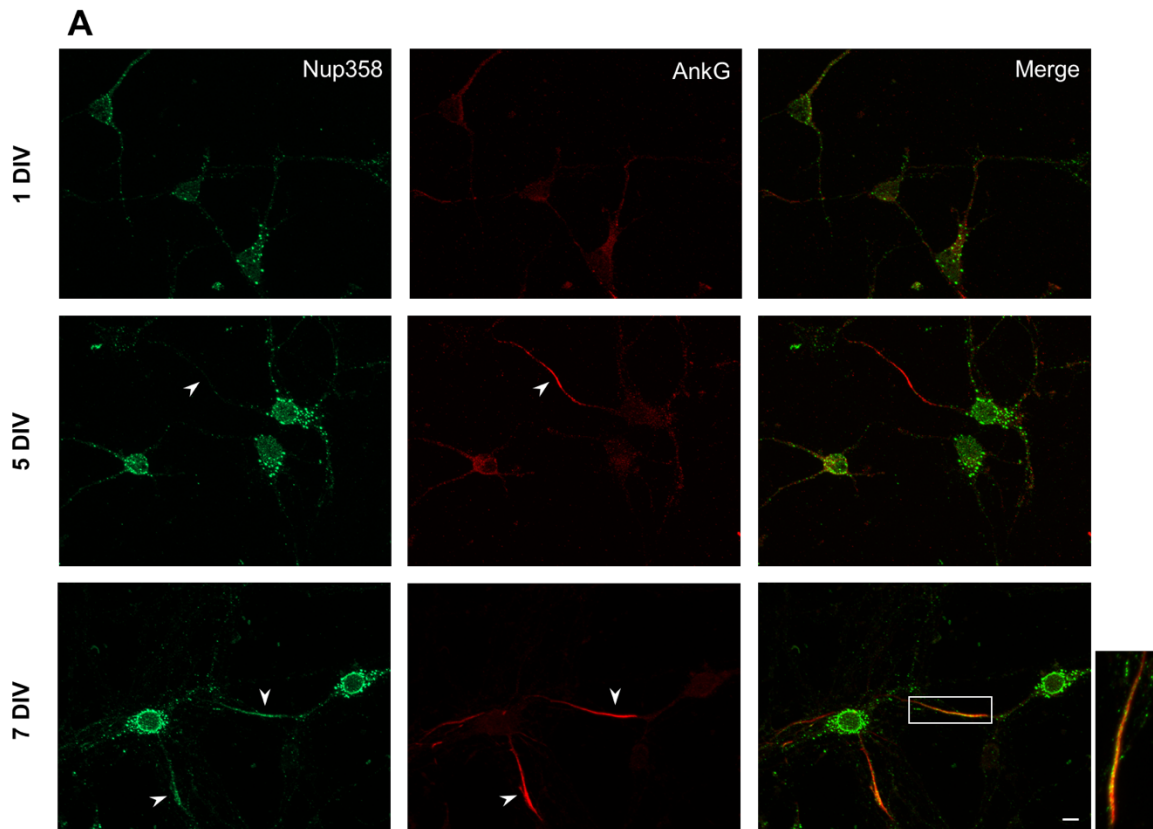
Although Nup358 localization in the ER and, generally, its spotted pattern in the cell body and neuronal processes were worth further investigation, these findings were beyond the scope of the present project. Instead, the focus was directed towards studying Nup358 localization at the AIS. To this end, Nup358 distribution pattern was examined in a time-dependent manner during the *in vitro* development of neurons,

including AIS maturation. Cultured mouse cortical neurons were fixed at different developmental stages (1-7, and 14 DIV) and co-immunostained for Nup358 and AnkG. Immunostaining for AnkG was chosen for two main reasons: 1) AnkG is one of the early markers of AIS formation ¹²⁷, and 2) AnkG is crucial for the concentration of other AIS proteins including voltage-gated sodium and potassium channels ^{134,135}, and the cell adhesion molecules NrCAM and neurofascin-186 ¹³⁶.

As early as 1 DIV, Nup358 was detected in the cell soma of cultured neurons, in the form of discrete spots (**Fig. 3-5, A; 1 DIV**). This spotted pattern was enhanced progressively during an increased period in culture correlating with neuronal development. At 5 DIV, when AnkG was noticeably recruited at the AIS of developing neurons, Nup358 was weakly detected at this specific region (**Fig. 3-5, A; 5 DIV**). A few days later in neuronal development, Nup358 was evident at the AIS and the perinuclear region, along with its spotted pattern in the cell soma and the rest of the neuronal network (**Fig. 3-5, A; 7 DIV**). Subsequently, in 14 DIV mature neurons, Nup358 was significantly more clustered at the AIS (see **Fig. 3-1**). At this stage of development, Nup358 distribution pattern was consisting of three identified fractions of the total pool: one fraction was localized at the nuclear rim, associated with NPCs, another fraction was present as discrete spots in the cell soma and processes, and a third fraction was enriched at the AIS along with AnkG signal. Collectively, these results demonstrate that the subcellular distribution of Nup358 changes relatively with neuronal development, and suggest that Nup358 clustering at the AIS is dependent on AnkG precedent localization in this region.

At the protein level, the temporal expression of Nup358 protein was assessed by immunoblotting homogenates of cortical neurons cultured for different time intervals, 7 to 21 DIV. In line with the immunocytochemistry analysis, the expression of Nup358 protein was increasing progressively during the development of neurons. This increasing trend was observed for a band of around 230 kDa MW, which is less than the reported MW of the mouse Nup358 protein, ~341 kDa, whose expression remained almost unchanged over the tested time course (**Fig. 3-5, B**). To have a wider frame for analysis during neuronal development, Nup358 protein expression was examined in mouse cortices obtained at different ages: at the embryonic stage E18 and during the postnatal

period P0-P90. The result was comparatively similar to that obtained with cultured neurons, showing an increased expression of the shorter isoform and an opposite gradual decrease in expression of the full-length Nup358 (**Fig. 3-5, C**). Next, I questioned whether the developmental changes in Nup358 protein expression were somehow paralleled by changes in expression of other nucleoporins. Hence, protein samples of mouse cortices were immunoblotted for the following nucleoporins: Nup153, Nup98, and Nup88. Surprisingly, a decrease was observed in expression of both Nup153 and Nup98 relatively as neurons develop, whereas expression of Nup88 was almost unchanged (**Fig. 3-5, D**). Therefore, both the immunocytochemistry and the Western blotting analyses infer a development-dependent change in not only Nup358 subcellular distribution in neurons but also in its protein expression of the two isoforms.



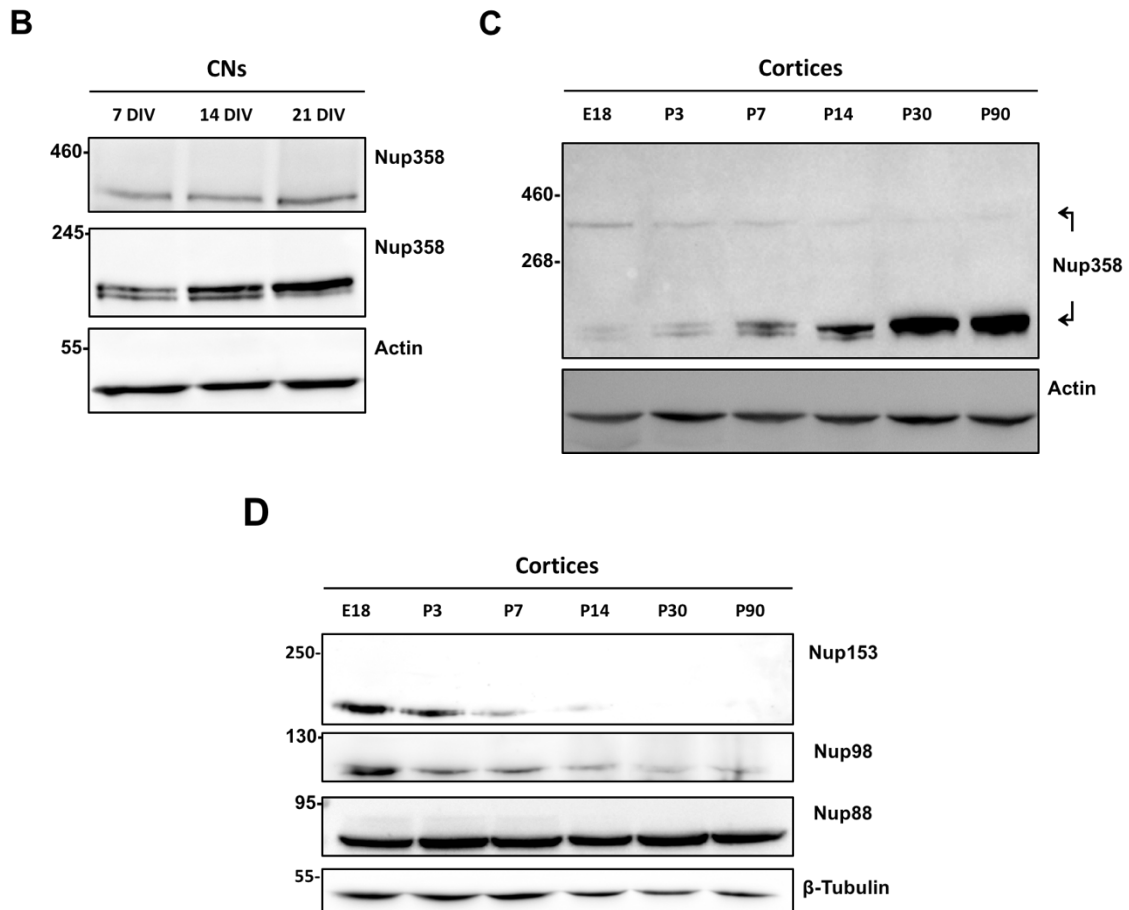


Figure 3-5 | Spatio-temporal expression of Nup358 during neuronal development. (A) Mouse cortical neurons were cultured for different DIV before being fixed and immunostained for Nup358 (green) and AnkG (red). At 5 DIV, AnkG expression is noticeable at the AIS, whereas Nup358 had a spotted pattern in the cell soma. At 7 DIV, Nup358 is detected at the nuclear rim and co-expressed with AnkG at the AIS. The arrowheads point to the recruitment of Nup358 and/or AnkG to the AIS. This is better demonstrated in the magnified view of the boxed area of the overlay image of the 7 DIV neurons. (Scale bar: 10 μ m). (B) Developmental expression of Nup358 protein in cortical neurons (CNs) cultured for different days in vitro. Note: the high MW Nup358 was weakly detected in cultured neurons so another antibody was used, that proved to have higher affinity for the 341 kDa band of Nup358. (C) Homogenates of mouse cortices of different ages were immunoblotted for Nup358. The full-length and the shorter isoforms of Nup358 have opposite trends varying gradually during neuronal development. The arrows point to the two isoforms of Nup358. (D) Western blot of mouse cortices showing developmental changes in the expression level of the nucleoporins: Nup153, Nup98, and Nup88. Both Nup153 and Nup98 decrease in expression during neuronal development, in contrast, no change was observed in the expression of Nup88.

3.4. Neurons express two isoforms of Nup358

Apart from a predicted 80 kDa isoform¹⁰⁵, no other isoform has been previously reported for Nup358. Thus, I aimed to verify the identity of the 230 kDa band as a shorter Nup358 using mass spectrometry (MS). Nup358 was immunoprecipitated from P30 mouse cortex and the sample was loaded on an SDS-PAGE gel; after which the gel was incubated with Coomassie stain to detect the 230 kDa band and finally analyze it

using MS (**Fig. 3-6, A**). The resulting analysis identified 40 unique peptides for Nup358, a number which is sufficient to confirm that the 230 kDa band belongs to Nup358. Interestingly, a few AIS proteins, including AnkG, have been identified as well with the shorter isoform of Nup358 (**Fig. 3-6, B**). However, no information was inferred from the MS data about the differences in protein sequence of the two isoforms, and how the shorter isoform is produced remains unclear. Though, it is tempting to speculate that there is a developmental switch in expression of the two isoforms of Nup358; consequently, the shorter Nup358 is assumed to be enriched at the AIS of mature neurons. To better identify which of the two isoforms of Nup358 is preferentially located in the nuclear rim or in the cytoplasm, including the AIS, a nucleo-cytoplasmic fractionation was conducted from 14 DIV neuronal lysate according to a previous protocol with minor modifications¹³⁷. The efficiency of fractionation was assessed by immunoblotting with the nuclear marker Lamin B1, and the cytoplasmic markers GAPDH and β -tubulin. The results obtained supported the hypothesis that the full-length Nup358 is enriched in the nuclear fraction, conversely, the shorter isoform is present in the cytoplasmic fraction (**Fig. 3-6, C**). Further, since Nup358 is part of the NPC present in the nuclear envelope, Nup358 might be expressed in virtually all eukaryotic cell types. Therefore, lysates of HeLa and NSC-34 cell lines along with 21 DIV neuronal lysate were immunoblotted for Nup358. In both cell lines, the expression of full-length isoform Nup358 was prevalent whereas in cultured neurons, the shorter isoform was preferentially expressed, thus, suggesting that the shorter isoform is a neuron-specific isoform of Nup358 (**Fig. 3-6, D**). N.B. Cultured neurons have weak expression of the full-length isoform, compared to cell lines, that can be detected using another anti-Nup358 antibody as in (**Fig. 3-5, B**).

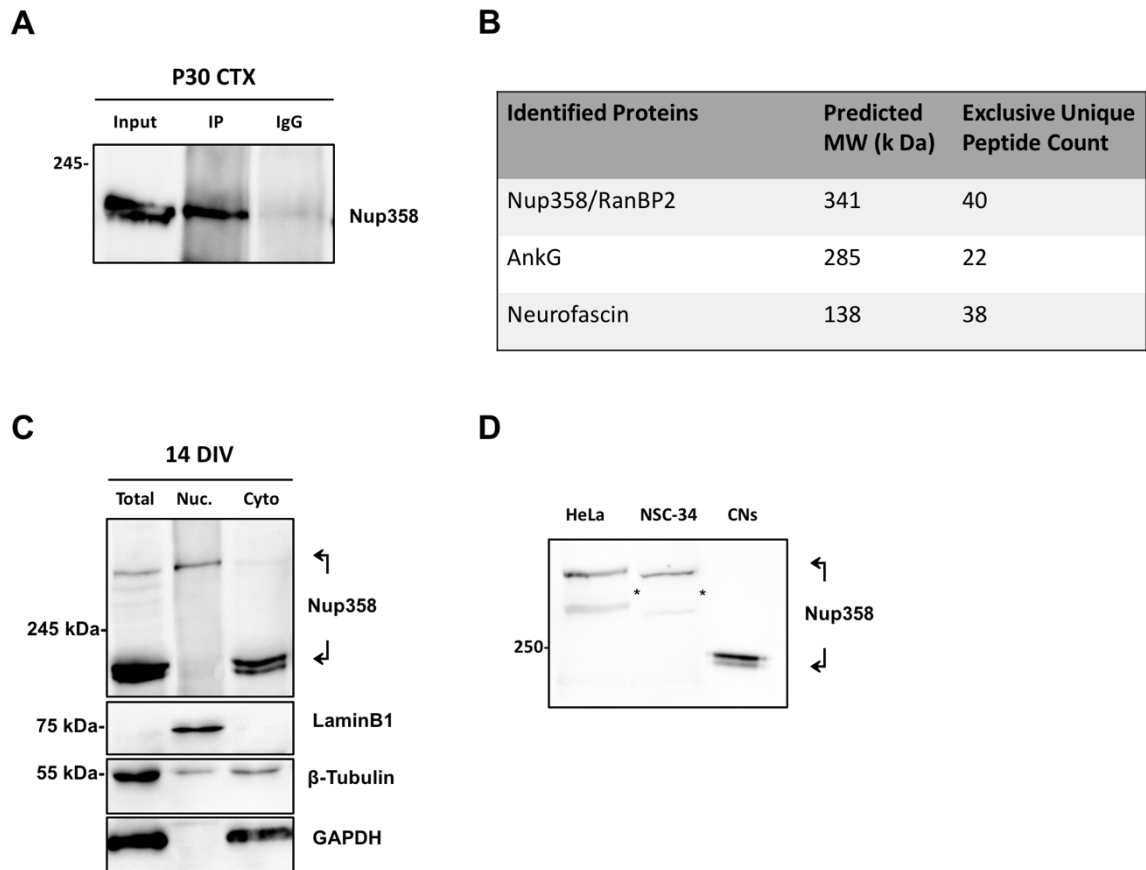


Figure 3-6 | Differential expression of Nup358 isoforms. (A) Immunoprecipitation of Nup358 from P30 mouse cortex to detect the 230 kDa isoform of Nup358. (B) Table highlighting the results of mass spectrometry analysis (of probability over 95%). Nup358/RanBP2 was identified in the immunoprecipitated sample together with AnkG and Neurofascin that are known to localize at the AIS. (C) Immunoblots of 14 DIV cortical neurons total lysate (total), the cytoplasm-enriched fraction (Cyto.), and the nuclear fraction (Nuc.). In the total lysate, both Nup358 isoforms were detected. In the nuclear fraction, the high MW isoform of Nup358 was detected, oppositely, the cytoplasmic fraction showed expression of the lower isoform. Lamin B1 was used as a nuclear marker whereas β -tubulin and GAPDH were used as cytoplasmic markers. (D) Lysates of HeLa and NSC-34 cell lines and 21 DIV cortical neurons were immunoblotted for Nup358. The arrows are used to point to the two isoforms of Nup358; bands marked with asterisks are probably non-specific bands.

3.5. Nup358 expression in different regions of the CNS

To examine the expression of Nup358 protein in different regions of the Central Nervous System (CNS), entire brain, hippocampus, cortex, and spinal cord were collected from mice at a fixed age, i.e. P3, and processed for Western blotting analysis. Equal amounts of protein samples were loaded on an SDS-PAGE gel and examined for their expression of Nup358 isoforms. Both isoforms were detected in all the tested tissues, with some variations in the expression level. In the brain, hippocampus, and cortex, expression of the full-length Nup358 was higher than that of the shorter isoform whereas the reverse result was observed in the spinal cord that has higher expression of

the shorter isoform (**Fig. 3-7, A**). These variations in expression levels of Nup358 isoforms are likely attributable to physiological differences among neuronal tissues.

Further, since the two isoforms of Nup358 are ubiquitously expressed in the CNS, changes in Nup358 expression levels were monitored during the development of both the hippocampus and the spinal cord. Similar to the developing cortex (see **Fig. 3-5, C**), both the hippocampus and the spinal cord showed an increased expression of the shorter isoform of Nup358 and a decreased trend in the full-length isoform (**Fig. 3-7, B**). Moreover, 14 DIV hippocampal neurons exhibited a distribution pattern of Nup358 similar to that of cultured cortical neurons (see **Fig. 3-1**), present localized in the perinuclear region, the cell soma and the AIS (**Fig. 3-7, C**). In contrast, glial cells such as astrocytes had a relatively less fluorescence signal of Nup358 compared to neuronal cells, as shown by the punctate pattern in the cytoplasm and at the nuclear rim (**Fig. 3-7, D**).

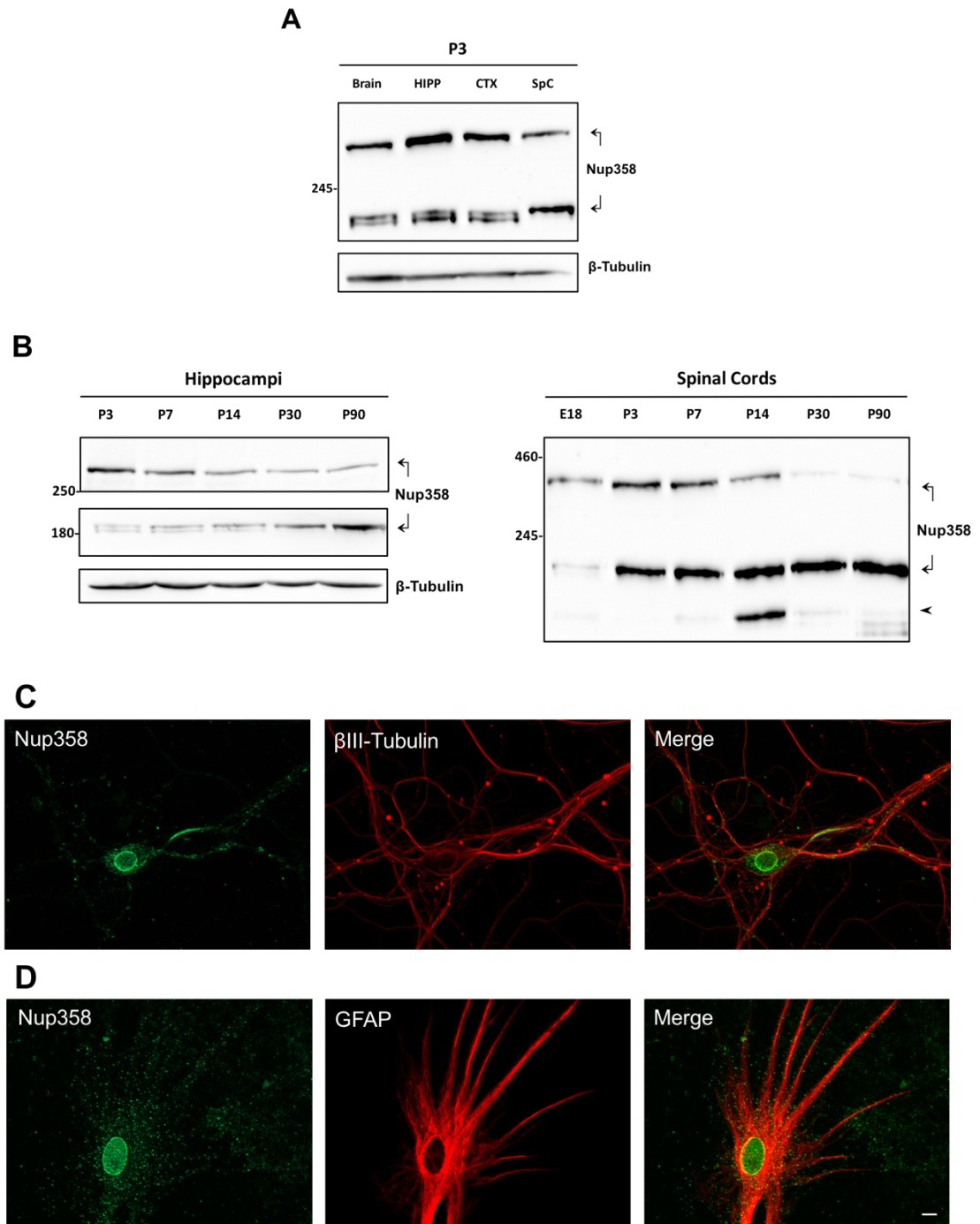


Figure 3-7 | Nup358 protein is ubiquitously expressed in the CNS. (A) Western blot of brain, hippocampus (HIPP), cortex (CTX), and spinal cord (SpC) obtained from P3 mouse. The two isoforms of Nup358 are commonly expressed in all the tested samples of neuronal tissues. (B) Development-dependent changes in Nup358 protein expression in hippocampi or spinal cords obtained from mice of different ages. Two antibodies were used for the detection of Nup358 isoforms since each antibody has a higher affinity for detecting one isoform. β -tubulin served as the loading control (in A and B). The arrows point toward the two isoforms of Nup358 having varying trends in expression during neuronal development. The arrowhead is directed toward an unidentified band observed in the P14 mouse spinal cord. (C and D) Immunofluorescent images of 14 DIV cultured hippocampal neuron and astrocytes immunolabeled for Nup358 and β III-tubulin in (C) or GFAP (glial fibrillary acidic protein) in (D) as a marker for astrocytes. Hippocampal neurons express Nup358 at the nuclear rim, the cell soma and the AIS

whereas astrocytes have Nup358 at the nuclear rim and in the entire cytoplasm as scattered spots. (Scale bar: 10µm).

3.6. The N-terminal region is essential for Nup358 clustering at the AIS

As Nup358 was found clustered at the AIS of mature neurons (see **Fig. 3-1**), I aimed to identify the region in its amino acid sequence essential for this specific localization. Neurons were transfected with GFP-co-expressing constructs that encode for different fragments of Nup358 protein. However, preliminary experiments were done in HeLa cell line to verify the efficiency of the constructs that encode for: the N-terminus of Nup358 (GFP-Nup358-N, 1-900 amino acid residues), the middle region (GFP-Nup358-M, 901-2219 residues) and the C-terminus (GFP-Nup358-C, 2220-3224 residues) (**Fig. 3-8, A**). The GFP-Nup358-N construct was expressed as filamentous structures surrounding the cell nucleus (**Fig. 3-8, B; GFP-Nup358-N**), presumably localizing at microtubules as previously reported¹¹¹ while the endogenous Nup358 was present in trace amounts at the perinuclear region and as scattered spots in the cell cytoplasm. As for the overexpression of the middle and the C-terminal regions, both showed a diffuse pattern but in contrasting locations in the cell. GFP-Nup358-M was preferentially localized inside the nucleus whereas the GFP-Nup358-C was expressed in the entire cytoplasm of HeLa cells (**Fig. 3-8, B; GFP-Nup358-M and GFP-Nup358-C**). In addition, transient transfection of the full-length Nup358 (GFP-Nup358-FL, 1-3224) was conducted as well, where results showed expression of the exogenous protein at the nuclear rim and the cytoplasm overlapping with fluorescence signal of endogenous Nup358 (**Fig. 3-8, B; GFP-Nup358-FL**).

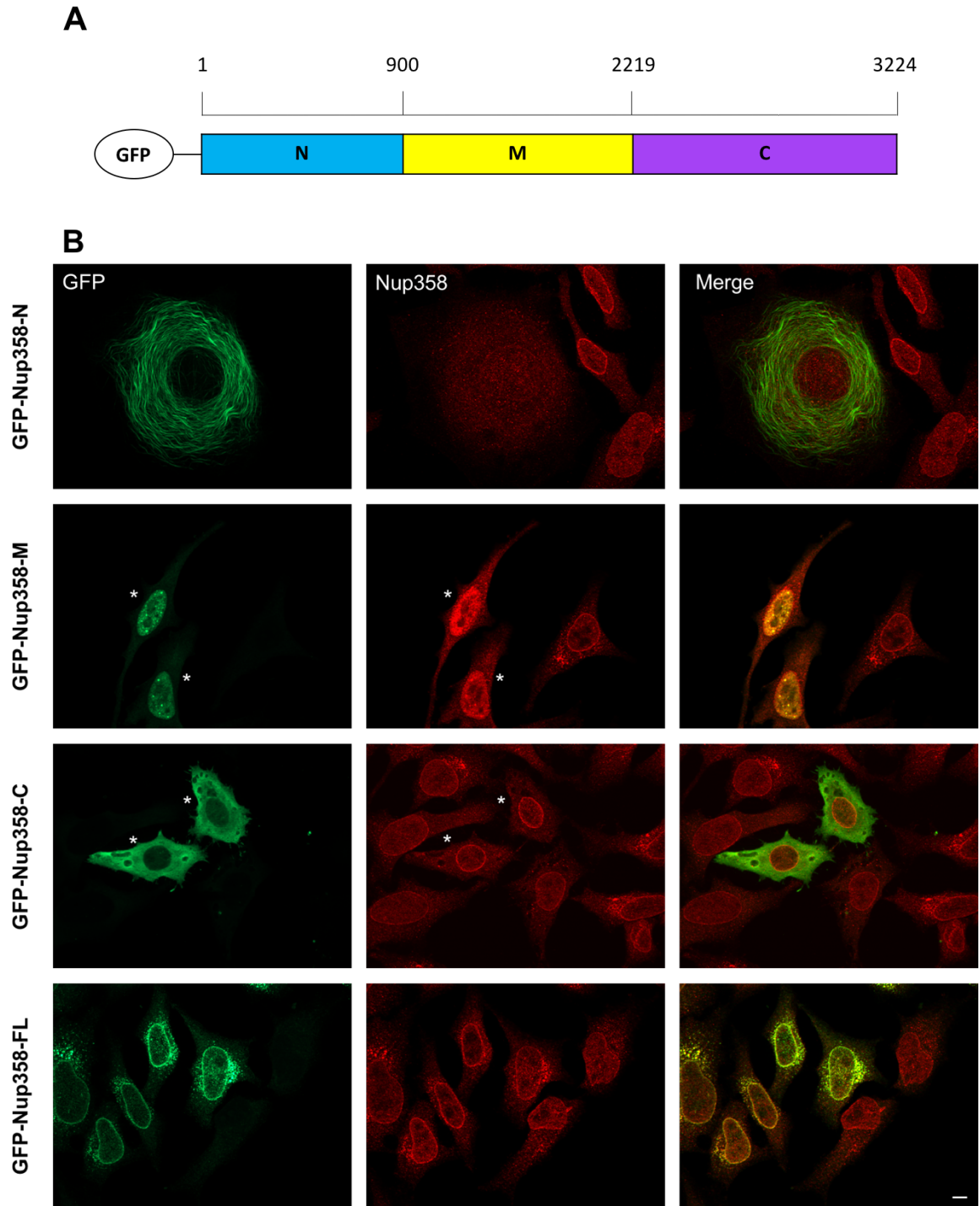


Figure 3-8 | Transient expression of Nup358 in HeLa cell line. (A) Schematic representation of human Nup358, composed of 3,224 amino acid residues, showing the different domains expressed by the constructs used in this study: The N-terminus (1-900 residues; blue), the Middle region (901-2219; yellow), and the C-terminus (2220-3224; violet). (B) Immunofluorescent images of HeLa cells transfected with GFP co-expressing constructs that encode for different regions of Nup358: GFP-Nup358-N (1-900 amino acids), GFP-Nup358-M (901-2219), and GFP-Nup358-C (2220-3224). Besides, HeLa cells were transfected with the construct GFP-Nup358-FL encoding for the entire human Nup358 protein (1-3224 amino acids). Transfected cells overexpress the N-terminus of Nup358 as filamentous structures surrounding the cell nucleus. The middle region is expressed preferentially inside the nucleus whereas the C-terminus is detected in the entire cytoplasm of transfected cells. Finally, exogenously expressed full-length Nup358 is

found around the cell nuclei and in the cytoplasm as punctate pattern. This distribution profile quite overlaps with that of endogenous Nup358 (red). (Scale bar: 10 μ m).

In a neuronal context, transfection of the Nup358 overexpressing constructs was primarily conducted in 10 DIV rat cortical neurons for around 16 hr, followed by fixation and immunostaining for Nup358. The GFP-Nup358-N was ectopically expressed along the microtubules cytoskeleton in all neuronal processes of the transfected neuron, indistinguishable between the axon and dendrites (**Fig. 3-9, A**). As for the endogenous Nup358, expression was limited to the spotted pattern in the cell soma without being detected in the nuclear rim or the AIS region. This result is, in fact, similar to that obtained in HeLa cell line (see **Fig. 3-8, B; GFP-Nup358-N**).

To examine a more specific subcellular profile for GFP-tagged Nup358, a hippocampal culture, which is a well-studied model of homogenous population of pyramidal neurons¹²², was used instead of cortical neurons. 13 DIV hippocampal neurons were transfected with the previously mentioned constructs, and maintained in culture for 2 days to allow expression of the exogenous protein. Then, neuronal cells were fixed and immunostained for AnkG to better identify the AIS and detect accordingly the co-localization with Nup358 at this specific region. In contrast to cortical neurons, hippocampal neurons exhibited a more distinct profile. GFP-Nup358-N was localized at the nuclear rim, in the cell soma and the AIS (**Fig. 3-9, B; GFP-Nup358-N**), in a pattern very much similar to that of endogenous Nup358. According to the present data, the N-terminus includes the amino acid sequence essential for Nup358 recruitment to the AIS of mature neurons. Regarding transfection with the other constructs, expression of the GFP-Nup358-M construct was unsuccessful in neurons, while expression of the GFP-Nup358-C construct resulted in a diffuse pattern in the cytoplasm of the neuronal cell (**Fig. 3-9, B; GFP-Nup358-C**).

Since Nup358 has two isoforms in neuronal lysates (see **Fig. 3-5, B**), one is full-length and the other is shorter, I examined the distribution pattern of GFP-Nup358-FL in neurons. 13 DIV hippocampal neurons were transfected, likewise, with the GFP-Nup358-FL construct and maintained afterward in culture for a 2-day period then fixed and immunostained for AnkG. Surprisingly, expression of the full-length Nup358 resulted in its localization solely at the perinuclear region without any signal at the AIS (**Fig. 3-9, B;**

GFP-Nup358-FL). To address possible relocation of exogenously expressed GFP-Nup358-FL, the incubation period was prolonged to 4 days' post transfection, yet the distribution profile was almost the same as in a shorter incubation period (data not shown).

The difference in the distribution pattern of endogenous Nup358 (or exogenous GFP-Nup358-N) and exogenous GFP-Nup358-FL might be related to the presence of the short isoform of Nup358 as observed in the Western blots (see **Fig. 3-5, B**). While the GFP-Nup358-FL construct includes the N-terminus region of Nup358 as in the GFP-Nup358-N construct, I assume that the short isoform of Nup358 has a more dynamic behavior in neurons and includes the N-terminus region sufficient for its clustering at the AIS. Indeed, investigating how the two isoforms of Nup358 are produced will be valuable to understand their dynamics and behavior in neurons.

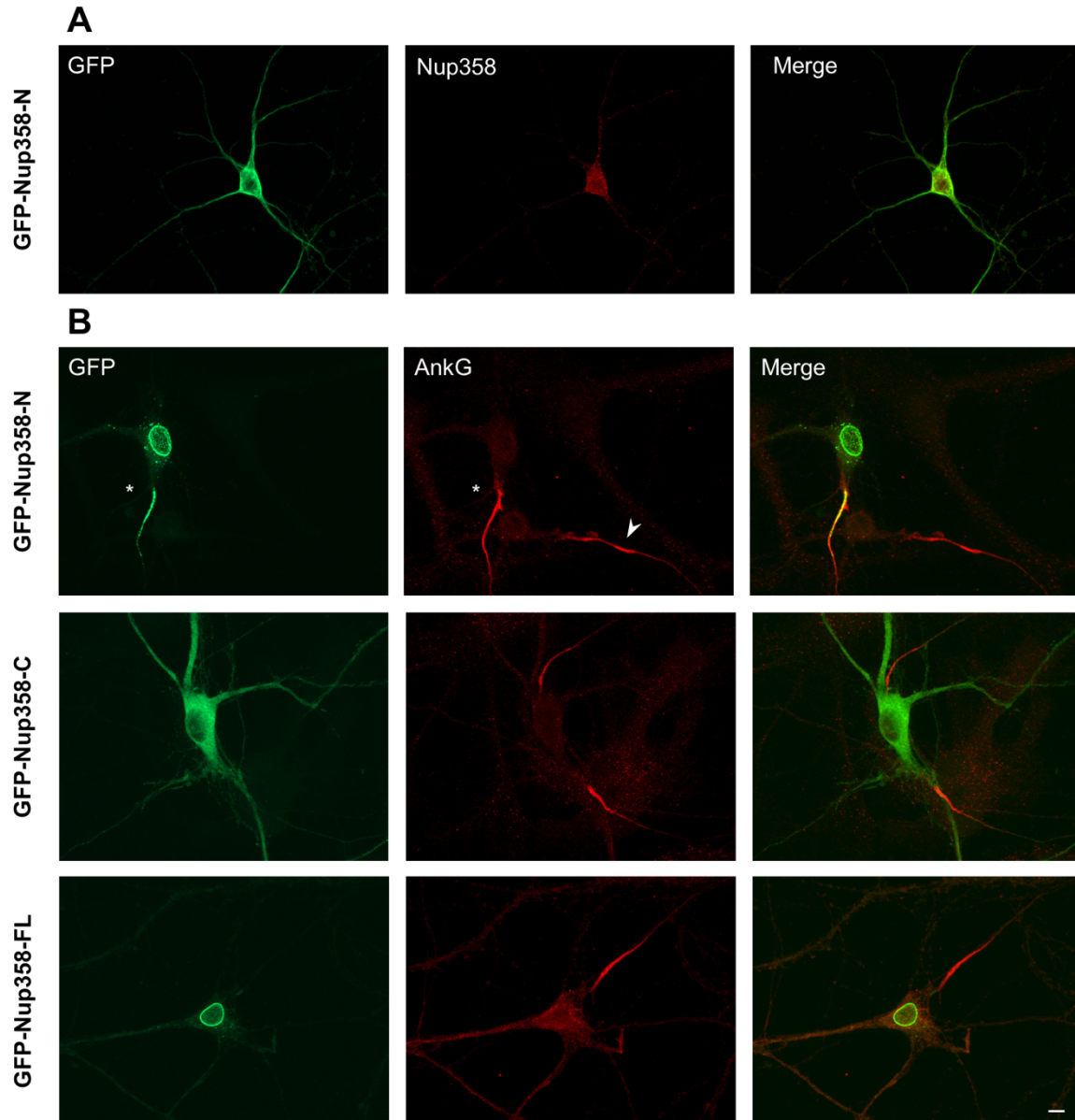


Figure 3-9 | Exogenous expression of Nup358 constructs in cultured neurons. (A) Rat cortical neurons were transfected with the GFP-Nup358-N construct at 10 DIV for around 16 hr, followed by fixation and immunostaining for Nup358 (red). Nup358 was expressed as filamentous structures in the processes of the transfected neuron. (B) 13 DIV rat hippocampal neurons exogenously expressing distinct domains of Nup358 and the full-length protein using constructs co-expressing green fluorescent protein (GFP): GFP-Nup358-N, GFP-Nup358-C, and GFP-Nup358-FL. Neurons were transfected at 13 DIV with the corresponding construct, fixed after 48 hr in culture and immunostained for AnkG to identify the Axon Initial Segment (AIS). Cells transfected with GFP-Nup358-N show expression of the N-terminal region at the nuclear rim and the AIS whereas cell transfected with GFP-Nup358-C show expression in the entire cytoplasm. Cells expressing GFP-Nup358-FL display a fluorescence signal around the nucleus. The asterisk and the arrowhead, in GFP-Nup358-N images, are used to mark transfected and untransfected neurons, respectively. (Scale bar: 10 μ m).

3.7. Activity-dependent decrease in Nup358 protein expression

Since Nup358 is enriched at the AIS that is the site of synaptic input integration and action potential generation, I aimed to study whether inhibiting or stimulating neuronal activity would trigger changes in Nup358 expression or distribution pattern. For this purpose, specific treatments were applied on 14 DIV cortical neurons, as neurons at this stage of development are fully mature and have already established functional synapses¹³⁸. The selected treatments included Tetrodotoxin (TTX) to block voltage-gated Na⁺ channels, Bicuculline (BIC) to block the inhibitory function of GABA_A receptors thus indirectly stimulating neurons, 4-Aminopyridine (4-AP) that blocks voltage-gated K⁺ channels therefore prolonging the action potential duration, and in some cases neurons were co-treated with BIC and 4-AP. Inhibiting neuronal activity with TTX did not interfere with Nup358 subcellular localization as compared with the control neurons (**Fig. 3-10, A**). The same result was observed with the BIC treatment; however, when neurons were treated with 4-AP, there was a decrease in the intensity signal of Nup358 (**Fig. 3-10, B**). This overall effect was more pronounced when neurons were treated with both BIC and 4-AP, showing a reduction in Nup358 intensity at the nuclear ring and the cell soma due to the synergistic effect of this combination of treatments.

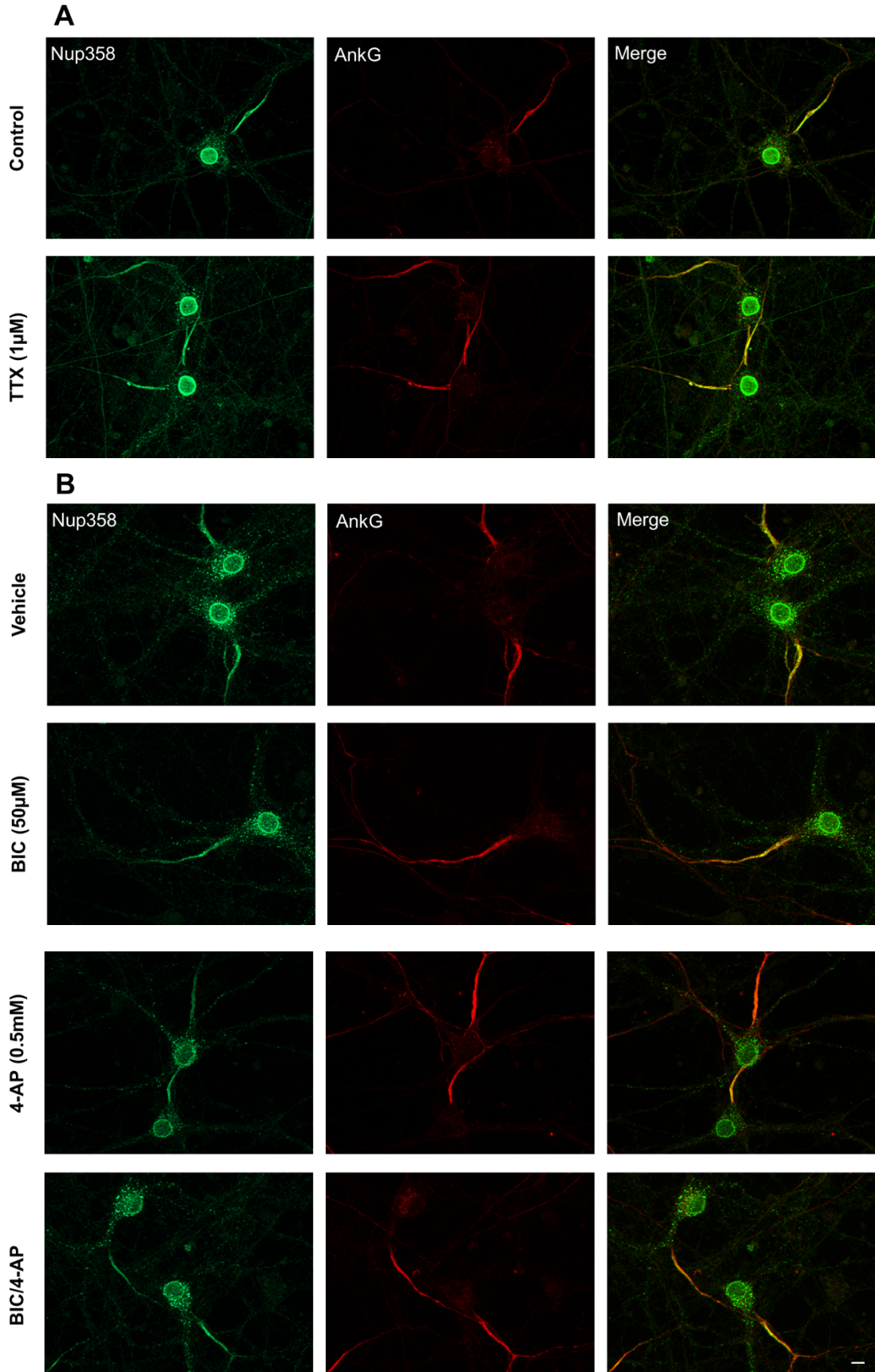


Figure 3-10 | Nup358 signal intensity is reduced following neuronal stimulation. Drug treatments were conducted overnight on 14 DIV cortical neurons to either inhibit or stimulate neuronal activity. (A) Cortical

neurons were treated with Tetrodotoxin (TTX; 1 μ M) to inhibit neuronal firing. (B) Bicuculline (BIC; 50 μ M) and/or 4-Aminopyridine (4-AP; 0.5mM) treatments were conducted to stimulate neurons. As a control, neurons were treated with an equivalent amount of DMSO (vehicle). Immunostaining was done for Nup358 and AnkG. A considerable decrease in Nup358 fluorescence intensity is observed when neurons were treated with 4-AP alone or in combination with BIC. (Scale bar: 10 μ m).

These observations were further confirmed by the quantitative analysis of Nup358 total fluorescence intensity using Operetta high-content imaging system; by which neuronal cells were detected with DAPI, which stains the cell nuclei, accordingly, Nup358 fluorescence intensity was measured in these cells (details are in the Materials & Methods section). Additionally, Nup358 fluorescence signal was measured at the level of the somatodendritic compartment (including Nup358 signal at the perinuclear region) and at the level of the AIS as identified by the overlapping signal of AnkG. A significant reduction was observed in Nup358 total fluorescence intensity following the treatment with 4-AP alone (\approx 15%) or in combination with BIC (\approx 30%) (**Fig. 3-11, A**). This result was paralleled by a reduction in Nup358 signal at the somatodendritic domain (**Fig. 3-11, B**), whereas at the level of the AIS, Nup358 signal remained unchanged (**Fig. 3-11**). Noteworthy that AnkG fluorescence intensity was not even changed compared to the control neurons (**Fig. 3-11, D**). This perhaps implies a robust stability of Nup358 (and AnkG) at the AIS region that is influenced by the complex AIS architecture and the interplay of various proteins in this highly-specialized region. Moreover, Western blotting analysis was conducted as well (**Fig. 3-11, E**) for neuronal lysates treated with BIC and/or 4-AP. Since the short isoform is the predominantly expressed isoform in 14 DIV neurons, the analysis was done relative to the 230 kDa Band of Nup358. Indeed, the results partially mirrored the immunocytochemistry quantitative analysis showing a significant decrease in Nup358 protein expression upon treating neurons with each of Bicuculline, 4-AP, or with both simultaneously. Overall, these data conclude that stimulation of neurons affects negatively Nup358 protein expression and distribution, however, Nup358 intensity at the AIS remains intact irrespective of the changes in the total pool of Nup358.

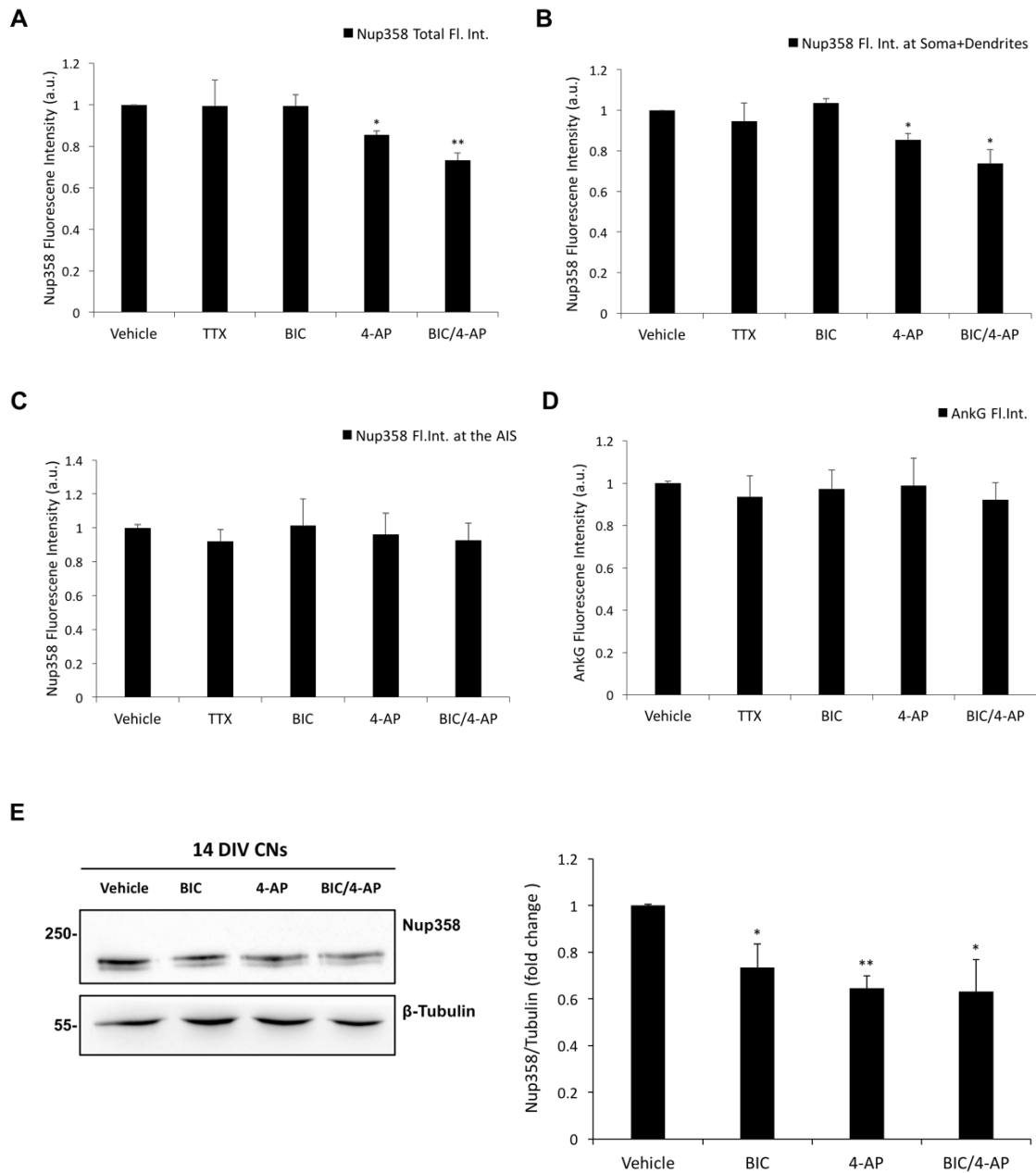


Figure 3-11 | Quantitative analysis of Nup358 fluorescence intensity following inhibition/stimulation of neuronal activity. 14 DIV mouse cortical neurons were treated overnight with each of TTX, BIC, 4-AP, BIC/4-AP or DMSO (vehicle) and immunostained for Nup358 and AnkG. (A) Measurements of Nup358 total fluorescence intensity (Nup358 total Fl. Int.). (B) Nup358 fluorescence intensity at the somatodendritic compartments (Nup358 Fl.Int. at Soma + Dendrites). (C) and (D) measurements of Nup358 and AnkG fluorescence intensity at the AIS of cortical neurons (Nup358 or AnkG Fl.Int. at the AIS). In (A-D) images were acquired using Operetta high-content imaging system and afterward analyzed with Harmony Software; the fluorescence intensity levels were normalized to the levels of the vehicle. (E) Nup358 immunoblot of neuronal lysates treated with BIC and/or 4-AP along with the quantifications of band intensity relative to β -tubulin as shown on the right of the blot. Bars indicate means \pm SD; n= 300-500 neurons from 21 different fields per experiment (the results presented are the mean values of three separate experiments) and wherever demonstrated, (*) or (**) represent significant values of $p < 0.05$ and $p < 0.01$, respectively. Statistical analysis was done using one-way ANOVA followed by Tukey's test.

3.8. Neuronal depolarization with KCl reduces Nup358 expression through Calcium influx and NMDARs

As demonstrated, the increased neuronal activity alters Nup358 subcellular distribution and dampens its protein expression. This link between neuronal activity and Nup358 distribution/expression was further studied by inducing neuronal depolarization with KCl, a commonly used treatment for stimulating neurons. Depending on the developmental stage, neurons convey KCl treatment into distinct signaling pathways that trigger local protein synthesis¹³⁸, overall increase in histone acetylation, gene-specific alternative splicing and increased chromatin accessibility¹³⁹, dendritic arborization^{140,141}, synaptogenesis and increased synaptic strength^{142,143}.

To examine how neuronal depolarization influences Nup358 subcellular distribution and protein expression, 14 DIV neurons were treated with KCl to a final concentration of 50 mM. Alternatively, neurons were treated with an equivalent concentration of NaCl as controls to maintain the osmotic concentration of monovalent ions. Assessment of cell death and neuronal integrity was done by staining cell nuclei with DAPI and the dendritic processes with MAP2.

Regarding Nup358 subcellular distribution, KCl-treated neurons showed a significant change in Nup358 profile noted by the loss of the sharp localization at the nuclear rim, whereas at the level of the AIS, Nup358 signal was persistent relative to AnkG staining (**Fig. 3-12, A**). In contrast, no change was observed in the NaCl-treated neurons. The reduction in Nup358 fluorescence intensity following KCl treatment was reflected in a decrease in its protein expression level, as shown by the Western blot analysis of KCl-treated neurons versus untreated neurons (**Fig. 3-12, B**). Theoretically, a decrease in protein expression might be modulated by an increased proteasome activity. To investigate such possibility, neurons were treated with MG132, a proteasome inhibitor, prior to the treatment with KCl. Indeed, immunoblotting showed that MG132 treatment did not recover Nup358 protein level following the treatment with KCl; thus, ruling out the role of proteasomes in the KCl-mediated decrease in Nup358 expression level (**Fig. 3-12, C**). Alternatively, the decrease in Nup358 protein might be a consequence of a substantial decrease in the mRNA level. To this end, qRT-PCR was conducted in KCl treated/untreated samples and *Nup358* mRNA was quantified and

normalized on *GAPDH* level (Fig. 3-12, D). Notably, the level of *Nup358* transcript was significantly reduced in neurons treated with KCl, therefore, neuronal depolarization with KCl triggers a decrease in both the protein and the mRNA levels of *Nup358*.

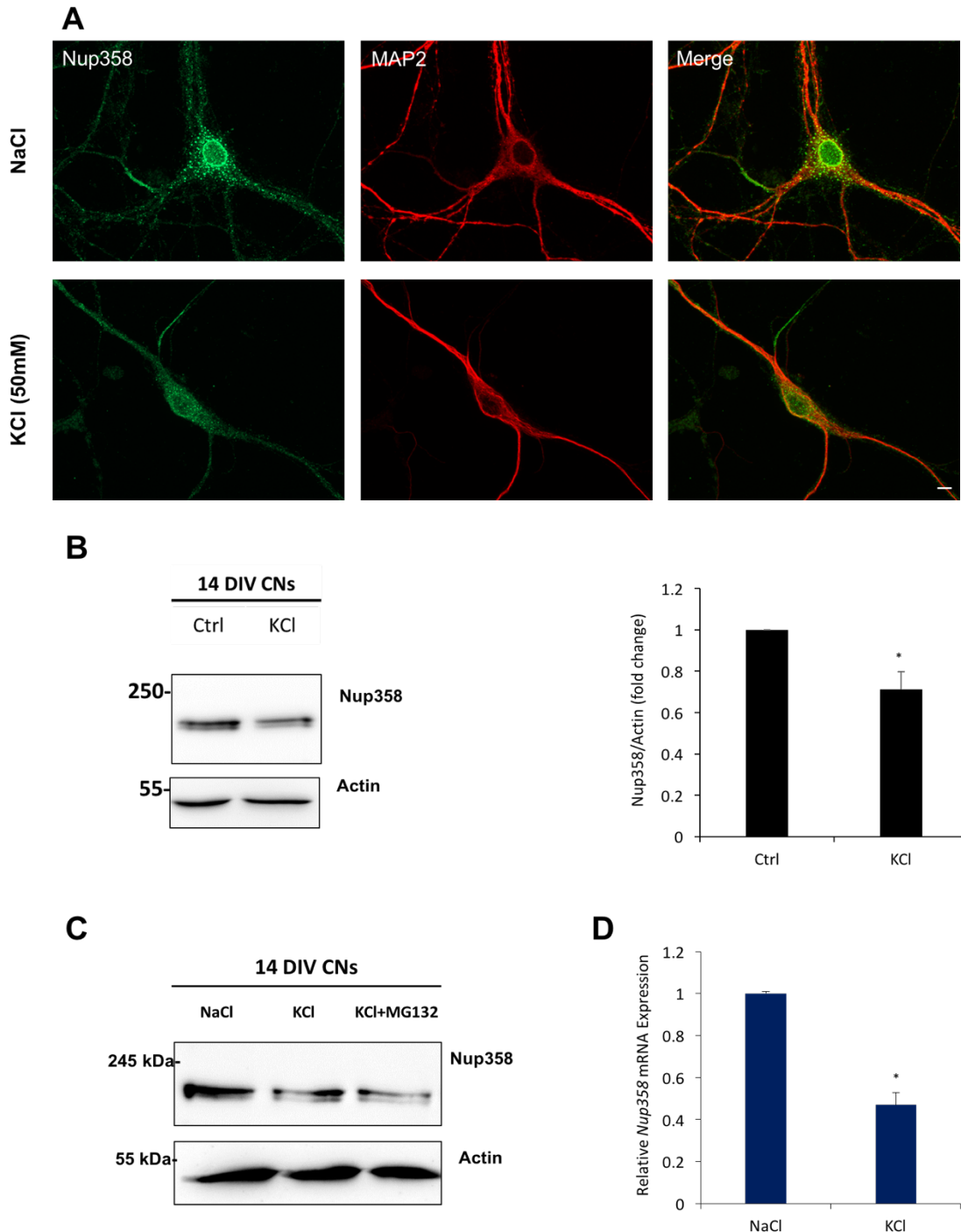
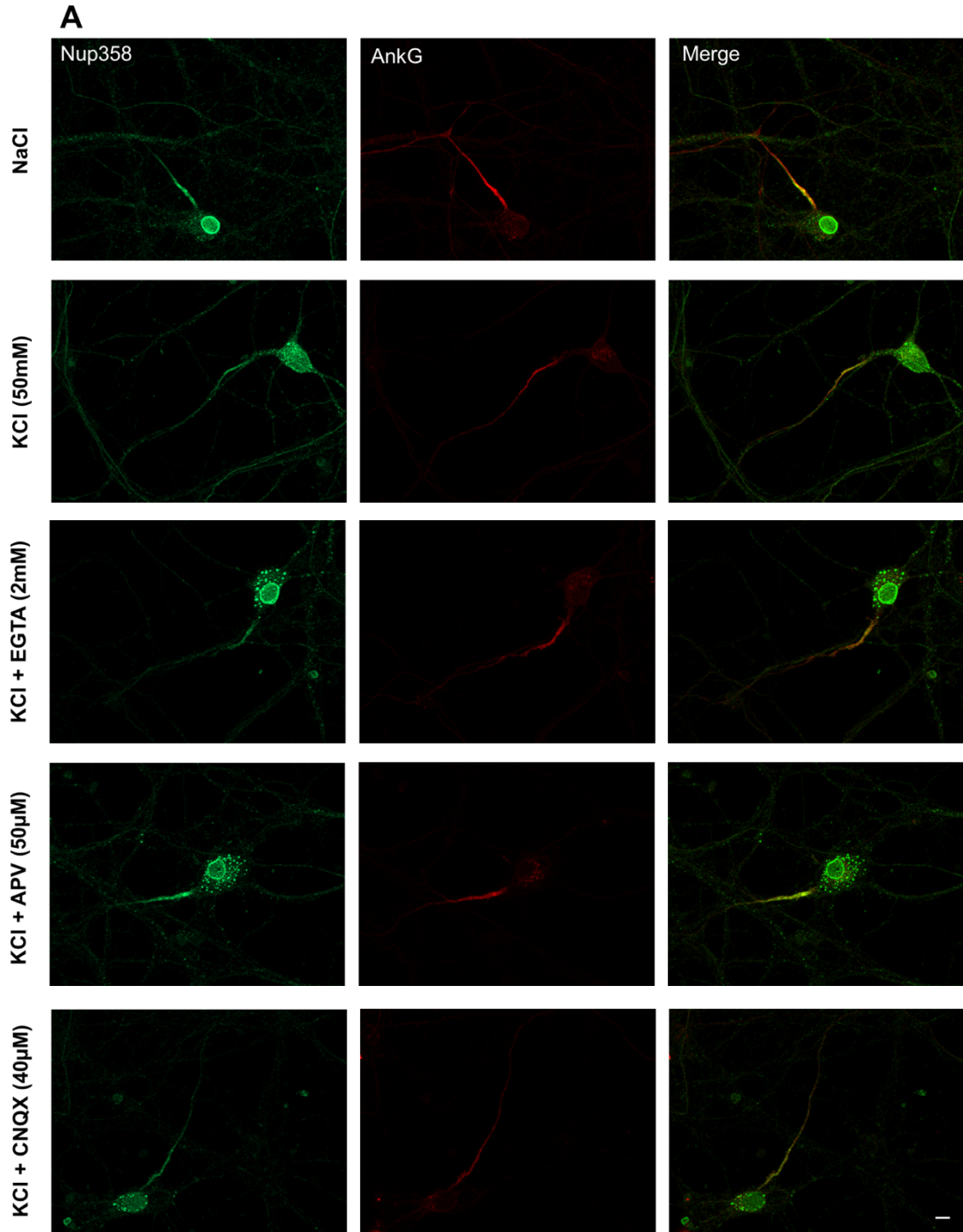


Figure 3-12 | KCl-mediated decrease in *Nup358* protein expression. (A) 14 DIV cortical neurons were treated with KCl at a final concentration of 50mM, and as control, neurons were treated instead with an equivalent concentration of NaCl. Immunostaining was done for *Nup358* (green) and MAP2 (red) to assess the cytoskeletal integrity of neuronal processes which was not compromised following the treatment. (Scale bar: 10µm). (B) Immunoblot of KCl-treated neuron lysates showing an approximate 30% reduction

in Nup358 protein level. On the right is the quantification of Nup358/Actin ratios in KCl-treated versus control neurons; where Actin served as the loading control. (C) 14 DIV neurons were pretreated with MG132 (1 μ M; overnight) and then with KCl (50mM, 1hr) to assess the role of proteasomes in KCl-mediated effect. Alternatively, neurons were treated with KCl alone, or NaCl to serve as controls. Compared to the control, both KCl- and KCl+MG132-treated neurons show reduced levels of Nup358 protein. (D) qPCR analysis showing a relative decrease in *Nup358* mRNA level in KCl-treated compared to the control neurons; normalization was performed on *GAPDH* mRNA level. Bars indicate means \pm SD and wherever demonstrated (*) or (**) represent significant values of $p < 0.05$ and $p < 0.01$, respectively. Statistical analysis was done using two-tailed Student's t-test.

To further investigate the KCl-underlying mechanism, certain drug treatments were applied on neurons to examine the rescue of Nup358 protein expression and/or distribution pattern. Thus, neurons were pretreated with: EGTA to block calcium entry, APV to block NMDA receptors, or CNQX that is an AMPA receptor antagonist. These treatments were selected since membrane depolarization and the subsequent increase in calcium influx, through voltage-gated calcium channels or NMDA/AMPA receptors induce various signaling pathways¹³⁸. Neurons were afterward processed for immunocytochemistry by staining for Nup358 and AnkG. Compared to control neurons and KCl-treated neurons, treatments with either EGTA or APV rescued Nup358 distribution pattern and fluorescence intensity (**Fig. 3-13, A**). However, the KCl/CNQX-treated neurons showed a low intensity signal for Nup358 and a distribution pattern similar to that of KCl-treated neurons. These results were confirmed with quantitative analysis of Nup358 total fluorescence intensity using Operetta high-content imaging system (**Fig. 3-13, B**). At the protein expression level, a partial recovery was observed when neurons were pretreated with EGTA whereas when blocking the NMDARs with APV, Nup358 protein expression was recovered (**Fig. 3-13, C**). Alternatively, the CNQX treated neurons showed Nup358 protein levels similar to that of the KCl-treated neurons (see **Fig. 3-13, C**). Noteworthy, that the full-length isoform was completely absent in the KCl, however, when neurons were treated with KCl/APV and KCl/EGTA, there was a relatively increased protein expression of the full-length isoform of Nup358. Altogether, these results imply that neuronal depolarization with KCl alters Nup358 overall expression, where the NMDARs and indirectly the calcium influx are involved in triggering this effect.



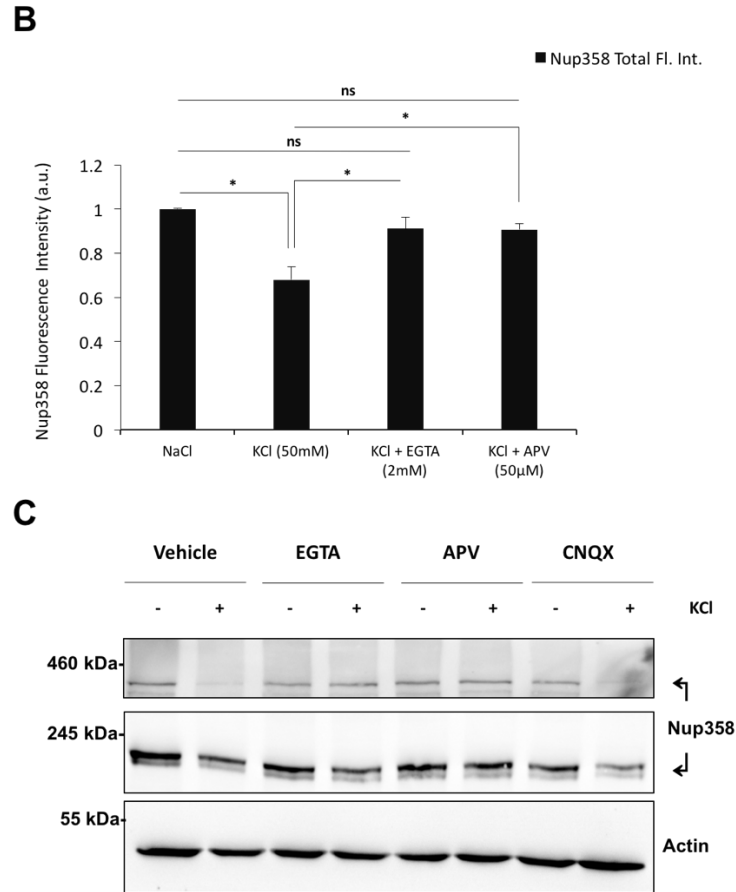


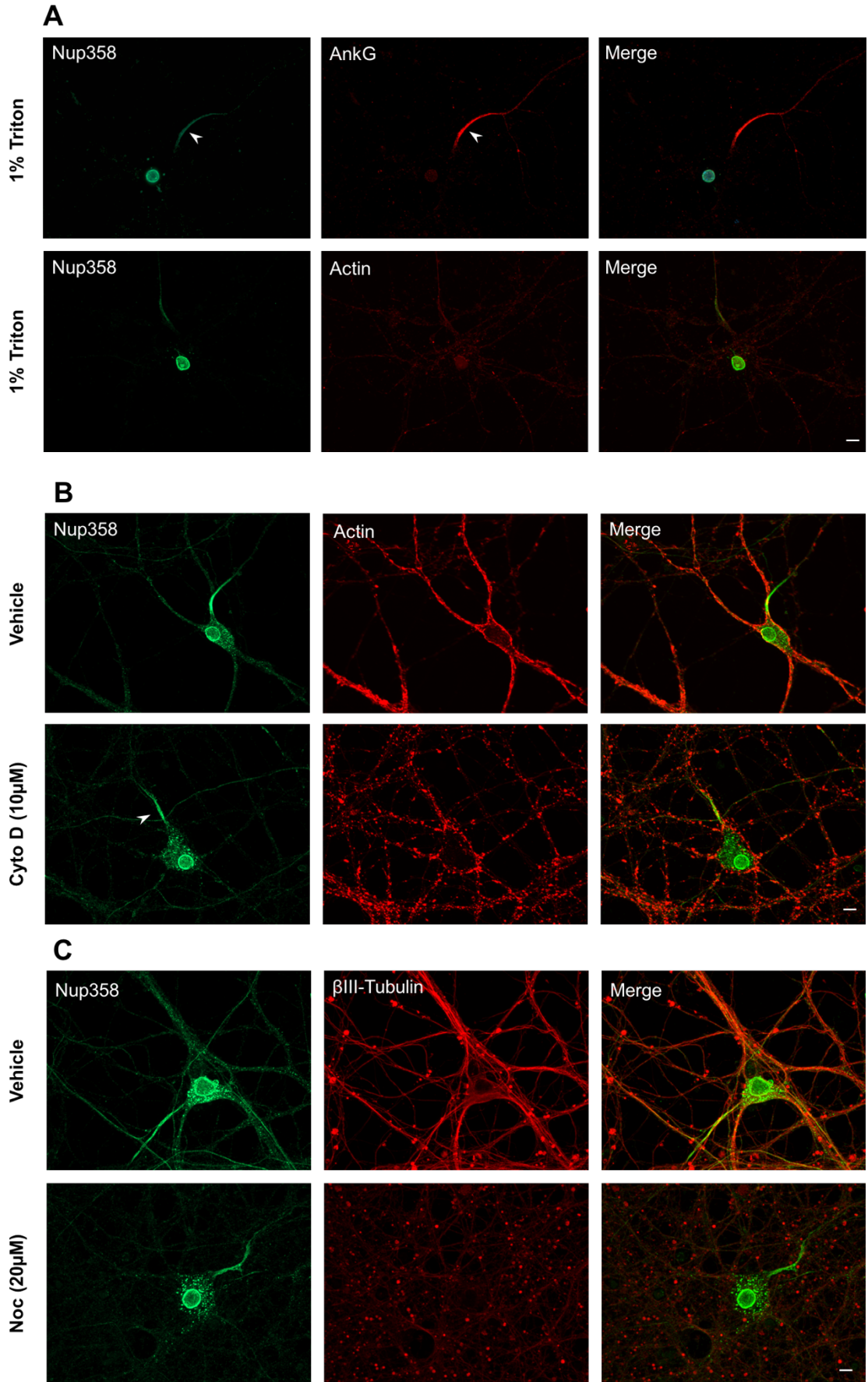
Figure 3-13 | KCl-triggered decrease in Nup358 expression is mediated by NMDARs. (A) 14 DIV cortical neurons were pretreated with: EGTA (2mM; 30 min), APV (50µM; 30 min) or CNQX (40µM; 30 min) followed by treatment with KCl (1 hr). Immunostaining was conducted for Nup358 (green) and AnkG (red). (Scale bar: 10µm). The immunofluorescent images show a recovery of Nup358 signal when neurons were treated with EGTA or APV prior to KCl. (B) Measurements of Nup358 total fluorescence intensity (Nup358 total Fl. Int.) using Operetta high-content imaging system showing Nup358 intensity values similar between the control neurons and the neurons pretreated with either EGTA or APV; additionally, when compared to the KCl-treatment, both EGTA and APV significantly recovered the KCl-dampening effect of Nup358 fluorescence. Bars indicate means \pm SD and wherever demonstrated (*), or (ns) represent significant values of $p < 0.05$ or not significant values, respectively. (C) Nup358 immunoblot for 14 DIV cortical neurons treated with KCl, and/or EGTA, APV, and CNQX; with Actin serving as the loading control. The arrows of Nup358 point to the two isoforms of Nup358, the full-length and the short isoforms. (-) or (+) marks are used to indicate where KCl was included or not in the treatment.

3.9. Nup358 localization at the AIS does not depend on actin-microtubule cytoskeleton

Nup358 is present at the nuclear rim and the cytoplasm through the association with NPCs⁸¹ and the ER, respectively (see Fig. 3-1 & Fig. 3-2). As the AIS represents a physical and physiological barrier for the mobility of molecules and proteins at the AIS^{126,144}, the high density of Nup358 protein at this region suggests a possible association with the AIS cytoskeleton. This hypothesis was evaluated through testing Nup358

resistance to non-ionic detergent extraction. Being insoluble to detergent extraction is a characteristic feature of most AIS proteins, due to either their direct association with the AIS cytoskeleton or, indirectly, through the interaction with scaffolding proteins at this region^{144,145}. To this end, 14 DIV mature neurons were treated with 1% Triton before being fixed and immunostained for Nup358 and AnkG; the results show persistent staining for Nup358, as well as for AnkG, indicating a potential interaction of Nup358 with the detergent-resistant AIS cytoskeleton/scaffolds (**Fig. 3-14, A**). As a positive control, detergent-extracted neurons were incubated with phalloidin, for identifying filamentous actin whose signal was significantly decreased (**Fig. 3-14, A**; lower panel).

Given the importance of the neuronal cytoskeleton in maintaining the AIS function^{146,147}, I examined whether altering actin filaments integrity by cytochalasin D (Cyto D) or disrupting microtubule polymerization by nocodazole (Noc) would affect the clustering of Nup358 at the AIS. While Cyto D treatment was sufficient to disrupt actin filaments in 14 DIV neurons, proved by the decrease in phalloidin staining when compared to control neurons (vehicle), Nup358 signal intensity at the AIS was remarkably unaffected (**Fig. 3-14, B**). In the same way, disrupting neuronal microtubules with Noc did not alter the distribution nor the expression of Nup358 at the AIS (**Fig. 3-14, C**). These observations were further confirmed by the quantitative analysis using Operetta high-content imaging system, that showed no difference in Nup358 fluorescence intensity between Cyto D- or Noc-treated neurons and the control neurons (vehicle) (**Fig. 3-14, D**). Altogether, these results imply that Nup358 localization at the AIS is not dependent on actin-MT neuronal cytoskeleton. Further, these data thus suggest that Nup358 is associated with an AIS scaffold protein, most likely AnkG.



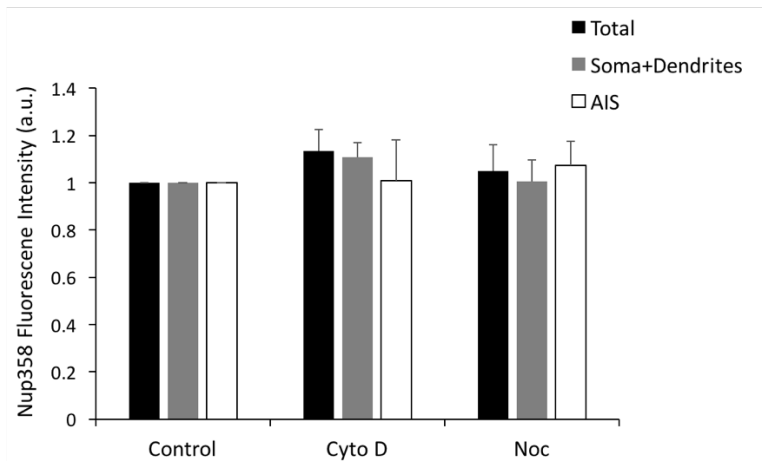
D

Figure 3-14 | Nup358 clustering at the AIS is not dependent on the actin-microtubule cytoskeleton. (A) 14 DIV cortical neurons were treated with 1%Triton in a cytoskeletal buffer before being fixed and immunostained for Nup358 (green) and AnkG (red). Control neurons were labelled instead for Actin using phalloidin staining (red). In both sets of images, Nup358 signal was persistent at the AIS as well at the nuclear rim, most likely due to its association with NPCs. (B) neurons were treated for 1 hr with Cyto D (10 μ M; 1 hr); disruption of actin filaments was monitored by phalloidin staining (red). (C) Depolymerizing microtubules was conducted by treatment with Noc (20 μ M; 3 hr), followed by fixation and immunolabeling with the microtubule marker β III-tubulin. In both (B) and (C), DMSO incubation was used as control (vehicle). (Scale bar: 10 μ m). (D) Quantitative analysis of Nup358 total fluorescence intensity, and at the level of the somatodendritic compartment and the AIS region, where results were almost identical with no significant difference between the CytoD- or Noc-treated neurons and the control ones. Bars indicate means \pm SD.

3.10. AnkG is required for Nup358 localization at the AIS

Based on the previous results presented in this study, I assumed that Nup358 localization at the AIS of mature neurons is dependent on AnkG, probably in a manner similar to other AIS proteins^{135,136,148}. AnkG is known to be the master scaffold protein present at the AIS that orchestrates the clustering of other AIS protein including Nav channels, KCNQ2/3, β IV-spectrin, and NrCAM (neuron-glia related cell adhesion molecule)^{135,149}.

To investigate the interdependence between Nup358 and AnkG for association at the AIS, either proteins were downregulated using RNAi method of GFP-coexpressing shRNA plasmids. As controls, neurons were transfected instead with a non-targeted shRNA. Transfections were conducted on 5 DIV mouse cortical neurons, afterward the medium was changed and neurons were maintained up to 10 DIV. Immunostaining was carried out with Nup358 and AnkG antibodies. Regarding transfection with the control shRNA, neurons demonstrated no change in Nup38 distribution profile or AIS assembly;

this was manifested by the normal staining of both Nup358 and AnkG (**Fig. 3-15**, top panel). As for assessing the ability of the shRNA in eliminating the expression of the target protein, the results show transfected neurons with a reduced signal of the corresponding protein. While as for testing the interdependence between Nup358 and AnkG, the results presented here show that upon downregulating AnkG, Nup358 was not recruited to the AIS region but present at the nuclear rim and in the cell soma, thus, proving the essential role of AnkG in the clustering of Nup358 at the AIS (**Fig. 3-15**, middle panel). However, surprisingly, Nup358 depleted cells exhibited a dramatic loss of AnkG signal compared to untransfected cells (**Fig. 3-15**, bottom panel), suggesting that Nup358 influences AnkG enrichment and/or stability at the AIS. Taken together, AnkG is a key scaffold for the recruitment of Nup358 and other AIS proteins at this region, however its long-term stability at the AIS might be related to a possible interaction with Nup358.

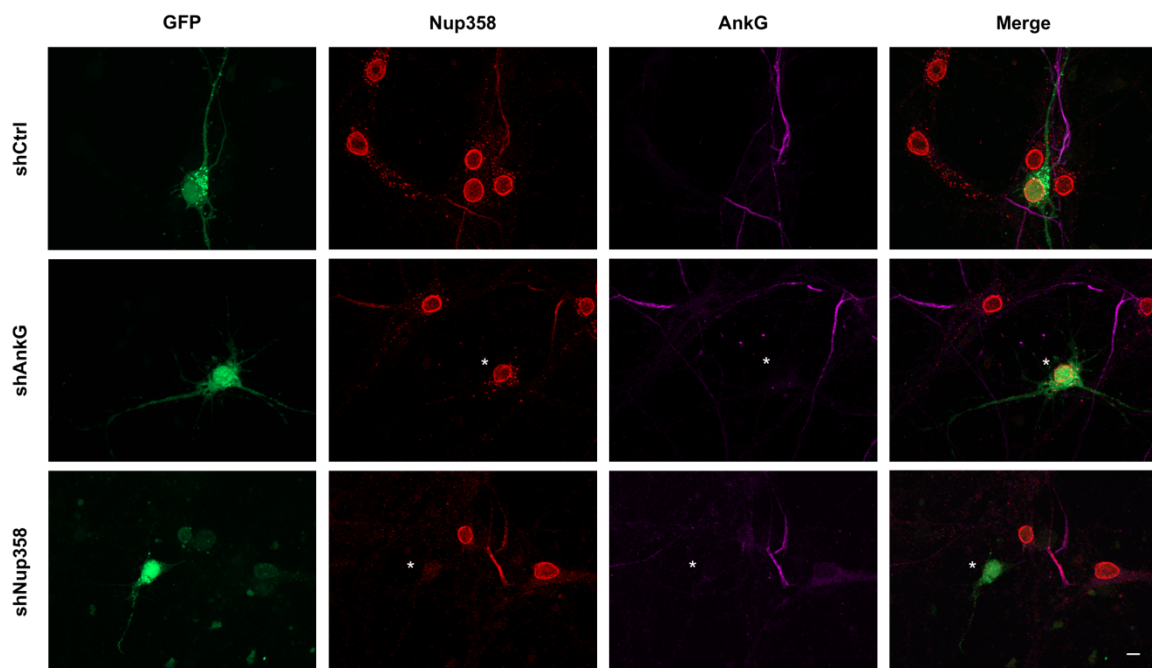


Figure 3-15 | Nup358-AnkG interdependence for enrichment at the AIS. Cortical neurons were transfected at 5 DIV with shRNA constructs co-expressing GFP to downregulate AnkG (shAnkG) or Nup358 (shNup358) and maintained afterward in culture up to 10 DIV. As control, neurons were transfected with non-targeted shRNA construct (shCtrl). Immunostaining was conducted for both AnkG (magenta) and Nup358 (red). Asterisks are used to mark the transfected neuronal cells (green) with a substantial decrease in both AnkG and Nup358 signals compared to the control untransfected cells. (Scale bar: 10µm).

4. DISCUSSION

Nup358 was initially described as a giant protein residing on the cytoplasmic filaments of the NPC^{81,82}. The classical role of this nucleoporin is then to contribute in the overall function of the NPC mediating nucleocytoplasmic transport; yet a few studies have identified Nup358 in the cytoplasm of various cell types. Since then, the dynamic behavior of this nucleoporin has been under the spotlight for subsequent investigations and in various cellular contexts including neuronal cells^{107,110,118,120}.

In this thesis, the key aim was to examine Nup358 role during the *in vitro* development of neurons that include establishing and maintaining neuronal polarity. As Nup358 was identified in the AIS of mature neurons, the central theme of the study was shifted towards addressing its clustering at this specific region and association with the AIS architecture. Further, I investigated the correlation between Nup358 and altered neuronal activity.

4.1. Unique subcellular distribution of Nup358 in cultured cortical neurons

In mature cortical neurons, Nup358 has a distinctive tripartite distribution pattern: present at the nuclear rim associated with NPCs, at the ER in the form of discrete spots, and clustered at the AIS (**Fig. 3-1**). At the nuclear rim, Nup358 localization was fairly expected; however, instead of having a punctate pattern relative to the NPCs traversing the NE at specific intervals (see **Fig. 1-1**), Nup358 formed an almost continuous ring around the nucleus. This is likely attributed to the high abundance of NPCs present in cultured neurons at this stage of development. And what supports this view is the similar trend observed when neurons were immunostained for different nucleoporins (**Fig. 3-3**). As the main role of NPCs is to mediate RNA and protein trafficking in neurons, the high abundance of NPCs in 14 DIV neurons might be linked to the relative metabolic activity of cultured neurons. This link between NPCs abundance and metabolic activity would need future investigations as little is known in this regard¹¹⁵ and generally little attention has been paid to the metabolic activity of cultured neurons¹⁵⁰.

As for Nup358 distribution in the cell soma, previous reports addressing Nup358 localization pattern showed that Nup358 associates with mitochondria in retinal cells

^{102,115}. However, in our model of cortical and hippocampal neurons, Nup358 is absent from both the Golgi apparatus and mitochondria (**Fig. 3-2**). Mitochondria staining in 14 DIV cortical neurons shows most COX1 fluorescence signal in regions that resemble dendritic protrusions (**Fig.3-2, C**), instead of being concentrated in the cell soma as commonly known. This might be related to the developmental stage of neurons including synapses/spines, and the movement of mitochondria to dendritic protrusions to accommodate for an increased energy requirements at specific sites ¹⁵¹. Above all, at 14 DIV, neurons are considered mature and already established synaptic contacts.

While Nup358 signal does not overlap with that of the mitochondria or the Golgi apparatus, the opposite is true with the ER signal. Localization at the ER is, however, specific for Nup358 among other nucleoporins that show restricted localization at the NPC with a trace signal present in the cell soma (**Fig. 3-3**). In fact, this result contradicts with a previous report claiming the presence of Nup358 together with other nucleoporins in the annulate lamellae of neurons ¹⁵². Annulate lamellae (AL) are membranous organelles that carry characteristic features of both the endoplasmic reticulum and NPCs. These AL structures are thought to be a reservoir for NPCs and are abundant in fast-growing cells to retrieve NPCs during cell division. Regarding neurons, there is controversy whether AL structures exist in such post-mitotic cells. According to the data presented here, nucleoporins-apart from Nup358-are barely detected in the ER, thus supporting the views against the presence of AL in neurons. Instead, these findings imply that the association with the ER is a unique feature of Nup358 among the rest of nucleoporins. Nup358 presence at the ER might supply neuronal cells with in response to physiological changes. Alternatively, Nup358 might be serving as a chaperone for specific proteins to the ER. In the neuroretina, for instance, Nup358 protein interact with the red and green opsin and modulate their subcellular localization in photoreceptors ¹¹⁶.

4.2. Two Nup358 isoforms

One major finding of this study was identifying two isoforms of Nup358 protein in neurons. Given that there is only one reported protein coding sequence for this gigantic protein, previous studies have detected Nup358 at varying molecular weights with no profound explanation about this discrepancy. My results of immunoblotting

samples of cortical neurons cultured for different periods, or alternatively homogenates of mouse cortices obtained at different ages, exhibit a gradual increase in a 230 kDa MW isoform of Nup358 whereas an opposite decrease was observed in the full-length Nup358 (**Fig. 3-5**). Further, the same trend for each isoform was observed in the hippocampus and the spinal cord during their development (**Fig. 3-7, B**) thus implying a general trend for expression of Nup358 isoforms in the central nervous system.

Based on the results of mass spectrometry analysis where the 230 kDa band was identified together with other AIS proteins, it is more likely that the shorter isoform of Nup358 is the isoform to be clustered at the AIS. Further, the results of nucleocytoplasmic fractionation of neuronal lysate showed an enrichment of the short isoform in the cytoplasmic fraction while the full-length Nup358 was predominant in the nuclear fraction (**Fig. 3-6, C**). Moreover, the increased expression of the short isoform correlates with the recruitment of Nup358 at the AIS of mature neurons (**Fig. 3-5, A-E**). All these data are accumulating evidence that the shorter isoform Nup358, rather than the full-length isoform, is enriched at the AIS.

Noteworthy that at an early stage of development, both the cortex and the hippocampus have a lower expression of the shorter isoform Nup358, as compared to the spinal cord. (**Fig. 3-7, A**). This variation might be related to physiological differences between tissues of the CNS such as differences in the AIS length among neurons obtained from each of the hippocampus, cortex and the spinal cord. Moreover, since the protein composition of the AIS and the nodes of Ranvier are very similar, Nup358 might be present at these regions as well and therefore the shorter isoform of Nup358 is consequently increased in expression in the long axon of motoneurons. Whether Nup358 is present at nodes of Ranvier or that motoneurons has longer AIS and more nodes than pyramidal neurons are key questions to address in the future for a better understanding about the behavior of Nup358 in different regions of the CNS. Indeed, it was previously reported that the loss of Nup358 in motoneurons causes the development of ALS-like syndrome; however, ALS-like symptoms were justified as a result of disrupted nucleocytoplasmic transport¹⁰³. With the current data showing Nup358 present at the AIS and further suggesting its presence at nodes of Ranvier,

Nup358 could be directly linked to neuronal excitability and therefore be implicated in neurological diseases.

Regarding the two isoforms observed, based on the data presented in this thesis, we cannot derive certain conclusions how the shorter isoform of Nup358 is produced; yet some speculations can be made that need to be supported by future experiments. One attractive scenario would be the presence of a switch in expression of Nup358 as neurons develop, where the shorter isoform is the predominant isoform. As many factors play role either positively or negatively to finely tune neuronal development, trans-acting factors could be one element that leads to this switch in expression of Nup358 isoforms. As a result, the possibility of having a spliced variant at advanced stages of neuronal development, encoding for the shorter isoform, would then be plausible. To get an answer for such a speculation, whether the production of the shorter isoform is due to a mRNA splicing event, better understanding of the mRNAs encoding both isoforms, through northern blotting technique, would be helpful in this case.

4.3. Nup358, a new player in the AIS architecture

The AIS is a unique highly-specialized region of the neuron morphology that has a central role in establishing neuronal polarity and modulating their excitability. It represents the site for synaptic input integration and action potential initiation. The AIS thus functions as both a physiological and physical bridge between the somatodendritic compartment and the axonal domain^{153,154}. Many reports have already identified its protein composition and interactions to maintain AIS integrity. The AIS represents a hub of Nav and Kv ion channels, cytoskeletal and scaffolding proteins¹⁴⁹. Of the AIS proteins, AnkG is the master regulator of the AIS architecture, essential for the AIS assembly, clustering of other AIS proteins and mediating their stability at this region^{134,136}

In this study, Nup358/RanBP2 has been identified in the AIS (**Fig. 3-1**). Since AnkG is of the early proteins that mark the AIS formation and is a key scaffold for the clustering of other AIS proteins, subsequent experiments were done to study the temporal expression of Nup358 relative to AnkG. Remarkably, as neurons develop in vitro, Nup358 clustering at the AIS lags behind that of AnkG; in other words, AnkG presence at the AIS might then drive the concentration of Nup358 to this exact region

(Fig. 3-5). Besides that, experiments were done to assess how Nup358 associates with the AIS architecture by disrupting actin cytoskeleton or microtubule polymerization. In either case, Nup358 localization at the AIS was unaffected thus suggesting an interaction with an AIS scaffold such as AnkG (Fig. 3-14, B and C). Moreover, AnkG was identified with Nup358 upon the immunoprecipitation the of Nup358 (Fig. 3-6, A and B). Thus, an interplay between Nup358 and AnkG could be a result of either a direct interaction or an indirect one modulated by another AIS protein. The hypothesis of Nup358-AnkG modulation was supported by the downregulation experiments showing a decrease in Nup358 expression at the AIS when AnkG was downregulated (Fig. 3-15). However surprisingly, depletion of Nup358 resulted in AnkG loss from the AIS region (Fig. 3-15). Most AIS proteins are dependent on AnkG for their association with the AIS whereas it was recently reported that AnkG-membrane partners, Nav channels and neurofascin-186, influence the stability of AnkG during the formation or maintenance of the AIS¹⁵⁵. Probably in the same manner, even though AnkG precedes Nup358 to recruit at the AIS, Nup358 is essential for the long-term stability of AnkG at this region; thus, suggesting an interdependence between both proteins for localization at the AIS. Further experiments would be needed to investigate whether Nup358 and AnkG are physically interacting with each other or that there is another mediator involved in this context.

Thus, in terms of function, Nup358 might serve as a scaffold for AnkG and other AIS proteins, however, Nup358 might be involved in neuronal activity as well. Upon stimulating neurons with 4-AP alone or when in combination with BIC, the overall expression of Nup358 was decreased (Fig. 3-10 and 3-11), while at the AIS Nup358 remained almost unchanged. Alternatively, when neurons were depolarized with KCl, a major reduction in Nup358 was detected at the AIS and in the entire neuronal cell (Fig. 3-12). While some treatment affect the expression of Nup358 only at the somatodendritic compartment, other treatments affect the expression of the total pool of Nup358 in all subcellular regions. This is a consequence of the different mechanisms induced by each treatment where the KCl-treatment induces calcium influx mediated by NMDARs, and substantially affects the mRNA level of Nup358.

4.4. Insight into the N-terminus domain of Nup358

As already demonstrated, the transient expression of the construct encoding the amino terminus region of Nup358 resulted in its localization at the AIS, as well as in the cytoplasmic and the perinuclear region. Whereas exogenous expression of the full-length resulted in restricted expression at the nuclear rim (**Fig. 3-8**). With this observation, I propose that the N-terminus is an essential region for Nup358 recruitment to the AIS. Despite that the GFP-Nup358-FL construct encodes for Nup358 protein including the N-terminal region, no signal was detected in the AIS. This perhaps implies that the shorter isoform lacks the sequence responsible for restricting Nup358 localization to the nuclear rim thus Nup358 has a more dynamic behavior in neurons and consequently is capable of clustering at the AIS.

Most AIS protein, such as Nav and Kv channels contain ankyrin repeat sequences that promote their interaction with AnkG and association with the AIS. However, the presence of ankyrin repeats is not crucial for localization at the AIS such as AnkB, one protein of the ankyrin family, which is not present at the AIS region but rather located in the distal region of the axon¹⁵⁶. In this regard, Nup358 amino acid sequence does not include such repeats though is capable of recruitment to the AIS. Following this further, some AIS proteins such as AnkG are associated with the AIS due to a post-translational modification as S-palmitoylation^{157,158}, hence are capable of binding to the plasma membrane. Interestingly, Nup358 protein sequence contains consensus sequences for palmitoylation and mainly located at the amino terminal region. Additionally, considering the different subtypes present in our model of cortical neuron culture, some neurons displayed localization of Nup358 close to the plasma membrane, especially at later developmental period. Despite that Nup358 is known to be a soluble protein and does not have transmembrane domains to allow integration in the plasma membrane, yet Nup358 has been visualized in the sub-membranous region of the AIS (**Fig. 3-14, B**). All in all, future examination of post translational modification on Nup358 protein sequence would be essential in understanding the mechanism of its clustering at the AIS of cultured neurons.

5. OUTLOOK

The dynamic behavior of Nup358 has been investigated, though poorly, in mammalian cell lines during both mitosis and the interphase period. In this thesis, Nup358 behavior has been examined in a neuronal context. Cortical and hippocampal neurons show a unique subcellular distribution of Nup358 that is not limited to its association with NPCs. Nup358 is present associated with the ER and most importantly, Nup358 clusters at the AIS of mature neurons. This localization at the AIS correlates with neuronal development and dependent on AnkG recruitment at this region. However, there is an interplay between Nup358 and AnkG for localization and/or long-term stability at the AIS. The protein sequence of Nup358 harbors multiple functional domains, capable of interacting with specific proteins. In this regard, the N-terminus region of Nup358 is crucial for clustering at the AIS. Moreover, Nup358 exists as two isoforms in neuronal cells; each isoform follow a certain trend relative to the stages of development. Collectively, these results underscore a non-classical distribution pattern of Nup358 in neurons with a focus on its localization at the AIS region.

However, future experiments are required to identify the mechanism of recruitment of Nup358 at the AIS. Direct interaction with AnkG or other AIS proteins might be one possibility. Additionally, post-translational modifications such as palmitoylation might also influence this specific localization. Concerning the two isoforms detected for Nup358, better knowledge about the mRNAs encoding for these isoforms will give an insight about the production of the shorter isoform and might be consequently linked to neuronal development.

As Nup358 is present in three fractions distributed in neuronal cells, the localization in the ER might be a store for Nup358 or that it acts as a chaperone for different AIS proteins. Understanding the dynamics of Nup358 is therefore essential to gain knowledge about the non-conventional roles for this nucleoporin. In terms of its functional role in neurons, Nup358 localization at the AIS might have a substantial influence on the overall activity of neurons; this aspect can be further addressed by downregulating Nup358 in neurons and examining its consequence on the action potential firing. Overall, the present study identifies a unique behavior of the

nucleoporin Nup358 in one of the most complex cells and further suggests its involvement in physiological or pathological neuronal conditions.

6. MATERIALS AND METHODS

While experiments were conducted by myself, Dr. Alessandro Roncador contributed in preparing the primary neuronal culture and Dr. Antonio Casini prepared the shRNA-AnkG construct.

Primary neuronal culture. Cortical and hippocampal cultures were prepared from E15 and E17 mouse embryos, respectively, using a previously described method¹⁵⁹ with some modifications. Briefly, cortices or hippocampi were dissected from C57BL/6 mouse brains and treated with papain solution [papain (20 U, Worthington), EDTA (5 mM), and Cysteine (30 mM) in 1X Earle's Balanced Salt Solution EBSS (Gibco)] for about 20 min in a 37°C water bath, with occasional swirling of the mixture. Complete dissociation of neuronal cells was achieved, mechanically, by gentle trituration through a serological pipette. DNase I (1 mg/ml, Sigma) was added to the neuron suspension and incubated for 3 min at 37°C. Then, cells were pelleted at 1,000 xg for 5 min, resuspended in an EBSS solution supplemented with bovine serum albumin (10 mg/ml, Sigma) and trypsin inhibitor (10 mg/ml, Sigma), and centrifuged again at 1,000 xg for 10 min. The pellet obtained was indeed resuspended in Minimal Essential Medium with Glutamax (Gibco) supplemented with 10% Fetal Bovine Serum (FBS), and plated on poly-D-Lysine (10 µg/ml, Sigma)-coated substrates. Cells were allowed to attach to the substrate in a humidified 37°C, 5% CO₂ incubator for 24 h, after which half the volume of the culture medium was replaced by Neurobasal Medium (Invitrogen) supplemented with 2% B-27 (Invitrogen) and AraC (5 µM, Sigma). Cultures were maintained up to 30 days *in vitro* (DIV), during which one half of the culture medium was replenished with fresh growth medium at 7, 14 and 21 DIV. Rat hippocampal cultures were prepared according to a previously described protocol¹⁶⁰.

Constructs. The plasmids used for the knockdown experiments were: scrambled negative control shRNA (shCTRL) and a pool of four mouse gene-specific Nup358 shRNA constructs (shNup358) in pGFP-C-shLenti Vector (Origene). The shAnkG target sequence, AGT TCA GAG GAA GTG AGT TAC, was retrieved from the RNAi Consortium (TRC) mouse shRNA library and the oligonucleotides were designed according to the TRC guidelines. The annealed oligonucleotides were then cloned into a pLKO.1 vector modified by

swapping the puromycin resistance gene with an EGFP expression cassette. For the transient expression of green fluorescent protein (GFP)-tagged Nup358 or its different fragments, the following constructs were kindly provided by Prof. Jomon Joseph¹¹¹: Full-length Nup358 (GFP-Nup358-FL; 1-3224 amino acid residues), N-terminal region (GFP-Nup358-N; 1-900 amino acids), Middle-region (GFP-Nup358-M; 901–2219 amino acids), and the C-terminal region (GFP-Nup358-C; 2220–3224 amino acids).

Transfections. Cortical neurons were transfected with the shRNA constructs using Lipofectamine LTX and Plus reagent (Invitrogen) according to the manufacturer's instructions with few modifications. In brief, 5 DIV cultured neurons were subjected to a medium change, though the old medium was collected and kept equilibrated in the 5% CO₂ incubator for later use. In one tube, 1µg of shRNA construct was diluted in 50µl Opti-MEM medium (Gibco) and 1µl of the Plus Reagent. In another tube, 1µl of Lipofectamine LTX was diluted in 50µl Opti-MEM. The shRNA & Plus mix was then added to the Lipofectamine mixture and incubated at room temperature for 5 min; this mixture was thereafter added per coverslip of 12-well tissue culture plates. Transfections were allowed to proceed for 2 h, after which the medium was replaced by one-half the volume of fresh growth medium and another half of the old medium. Transfected neurons were maintained in culture up to 10 DIV, then fixed with 4% PFA and processed for immunofluorescence. For the transient expression of GFP-Nup358-FL, GFP-Nup358-N, GFP-Nup358-M and GFP-Nup358-C, transfections were performed using calcium phosphate protocol¹⁶¹. Rat hippocampal neurons were transfected at 13 DIV then maintained in culture for 48-96 h to allow expression of the exogenous protein. Instead, for transfecting HeLa cells, Viafect reagent (Promega) was used according to the manufacturer's instructions and expression was allowed for 48 h in Dulbecco's modified Eagle's Medium (Gibco) supplemented with 10% FBS and 1% Penicillin/Streptomycin at 37°C in a humidified 5% CO₂ incubator.

Pharmacological treatments. To test whether inhibiting transcription affects Nup358 distribution profile, neurons were treated with either actinomycin D (ActD; 5µg/ml) or DMSO (vehicle) as a control for 1 h, along with 5-Ethynyl Uridine (EU; 0.5 mM, Thermo Fisher Scientific), a Uracil analog that gets incorporated into nascent RNA

during transcription. As for the detergent extraction experiments, cultured cortical neurons were washed briefly with a pre-warmed HBSS, then incubated with 1% Triton X-100 in the cytoskeletal buffer (2 mM MgCl₂, 1 mM EGTA, 60 mM PIPES buffer pH7.0) for 5 min at 37°C, followed by fixation and immunostaining¹⁴⁴. To study the association of Nup358 with the neuronal cytoskeleton, selected drug treatments were carried out to perturb either actin filaments or microtubules. To depolymerize actin filaments, neurons were treated for 1h with cytochalasin D (Cyto D; 10µM, Sigma) whereas to disrupt microtubules, neurons were treated for 3h with nocodazole (Noc; 20µM, Sigma). Alternatively, neurons were incubated with DMSO alone (vehicle) to serve as negative control. To address the influence of neuronal activity on Nup358 protein expression and distribution profile, the following treatments were conducted overnight: Tetrodotoxin (TTX; 1µM, Sigma), Bicuculline (BIC; 50µM, Sigma), 4-Aminopyridine (4-AP; 500µM, Sigma), and in some cases, neurons were co-treated with BIC and 4-AP, simultaneously. Depolarization of neurons was carried out for 1 h by adding KCl to a final concentration of 50 mM in complete Neurobasal Medium and wherever mentioned the KCl-treatment was preceded by an incubation for 30 min with any of EGTA (2mM), APV (100µM, Sigma) or CNQX (40µM, Santa Cruz Biotechnology). Following these treatments, neurons were fixed and processed for immunocytochemistry; otherwise, neurons were lysed and prepared for Western blotting or subjected to RNA extraction for qRT-PCR. All these treatments were conducted on 14 DIV cortical neurons.

Antibodies. The primary antibodies employed in immunofluorescence included: two closely related rabbit anti-Nup358 that recognize a region between 1050-1100 of the amino acid sequence (1:100, Abcam & Bethyl), mouse anti-Nup88 (1:100, Santa Cruz Biotechnology), mouse anti-Nup98 (1:100, Santa Cruz Biotechnology), mouse anti-m414 (1:100, Abcam), mouse anti-AnkG (1:100, Neuromab & Thermo Fisher Scientific), mouse anti-MAP2 (1:500, Sigma), mouse anti-βIII-Tubulin (1:300, Sigma), mouse anti-Golgi P58 (1:100, Sigma), mouse anti-COX1 (1:100, Abcam), mouse anti-Calnexin (1:100, Abcam), mouse anti-GFAP (1:100, Abcam),. The corresponding secondary antibodies were 488-, 594-Alexa-conjugated (1:800, Invitrogen), and 647-Alexa-conjugated (1:100, Abcam). For Western blotting, the following antibodies were included: mouse anti-Nup358 (Santa Cruz Biotechnology) against the amino acid sequence 1-300 of the N-terminus, mouse

anti-Actin (Abcam), mouse anti-Nup153 (1:100, Abcam), mouse anti-GAPDH (Santa Cruz Biotechnology), rabbit anti- β -Tubulin (Cell signaling), and goat anti-Lamin B1 (Santa Cruz Biotechnology).

Immunocytochemistry. Treated/untreated neurons were washed with prewarmed HBSS and fixed with 4% PFA for 15 min at room temperature. After fixation, cells were rinsed three times with PBS, 5 min each, and immunofluorescence was carried out as follows: neurons were permeabilized with 0.1% Triton X-100 in PBS for 10 min, then incubated with the blocking solution (2% BSA, 2% FBS, 0.2% Gelatin in PBS) for 1h at room temperature. Incubation with primary antibodies was done overnight at 4°C, subsequently, incubation with the relative Alexa fluor-conjugated secondary antibodies was carried out for 1 h at room temperature. Phalloidin staining was performed as previously described¹⁶¹. Nuclei were stained with DAPI for 10 min; coverslips were then mounted using Mowiol and allowed to dry overnight at 4°C. For the detection of 5- EU (5-ethynyl uridine), click chemical reaction was conducted on fixed neurons after the blocking step, using 10 μ M of the fluorescent label 5-FAM-Azide (5-FAM, Jena Bioscience) in the following solution (100 mM Tris pH 8.5, 1 mM CuSO₄, 100 mM ascorbic acid) for 30 min. Afterwards, neurons were washed three times in TBS buffer with 0.5% Triton X-100, followed by immunostaining for Nup358 as described before.

Imaging. Microscopic analysis was performed using the 63x oil objective of the Zeiss Observer Z.1 microscope, equipped with the ApoTome.2 module. Images were acquired and processed into orthogonal projections of 15-20 optical z-planes (0.24 μ m interval), using ZEN 2 imaging software (Zeiss).

High-Content Analysis. Cortical neurons (60,000 cells/well) were plated in 96-well Cell Carrier plates (PerkinElmer) and allowed to grow up to 14 DIV, the day at which drug treatments were conducted. Neurons were fixed and immunolabeled for Nup358 and AnkG as described previously. Nup358 fluorescence intensity of treated and untreated neurons were measured using the Operetta High-Content Imaging System (PerkinElmer). To maximize the accuracy of this quantitative analysis, each condition was conducted in five replicate wells, of which at least 18 fields were selected per well. Images were acquired using the 40x objective, and analyzed with Columbus 2.2

software. Neuronal cells were detected through nuclei staining with DAPI, and segmentation of the neuronal network was achieved by applying a combination of algorithmic parameters. This segmentation, therefore, allowed for a comprehensive analysis of Nup358 fluorescence intensity at the level of the AIS (marked by AnkG staining) and the somatodendritic compartment, in addition to a total intensity value (summation of both AIS and somatodendritic values); all measurements were corrected by subtracting the background intensity.

Western blotting. To analyze changes in Nup358 protein expression during neuronal development, cultured neurons were collected at different DIV. Cells were washed briefly with ice-cold PBS, then scraped and lysed in CHAPS lysis buffer [0.5% CHAPS (Sigma), 1 μ M EDTA, 150 μ M NaCl, 50 μ M Tris-HCl pH 7.4, 10% glycerol, and protease inhibitor cocktail (Roche)]. Alternatively, tissues were dissected from mice at the embryonic day (E18) and during the postnatal period (P3-P90). Mouse cortex, hippocampus and spinal cord were isolated and homogenized using the same lysis buffer. Homogenization of tissue samples was conducted using a motor driven homogenizer (Heidolph), by applying 10-15 strokes at 1,000 RPM in a glass tissue grinder. Cell lysates or crude tissue homogenates were then centrifuged at 10,600 xg for 10 min at 4°C. The supernatant of each sample was collected and equal amounts of protein were loaded on a 5-8% gradient SDS-PAGE gel. Prior to protein transfer onto a nitrocellulose membrane (GE Healthcare Sciences), the SDS-PAGE gel was rinsed for 2 min in the fixing solution (40% methanol, 10% acetic acid, 50% Milli-Q water). Transfer was carried out overnight at 4°C, at low voltage (40V), and immunoblotting was proceeded according to standard protocols. For the nucleocytoplasmic fractionation experiment, the total lysate of 14 DIV cortical neurons was obtained by using the previously mentioned buffer, CHAPS buffer. Alternatively, neurons were lysed according to the protocol¹³⁷ to isolate the cytoplasmic-enriched fraction using STEN buffer and the nuclear-enriched fraction using RIPA buffer. In all buffers, protease inhibitor cocktail was included.

Immunoprecipitation. Immunoprecipitation of Nup358 was performed using homogenates of P30 mouse cortices. 2 μ g of rabbit polyclonal anti-Nup358 was

incubated with 500µl of the tissue homogenate overnight at 4°C, while 2µg of rabbit normal IgG antibody was used instead as a control. Afterwards, 30µl of Dyna Protein A magnetic beads (Invitrogen) were washed once with the ice-cold CHAPS lysis buffer and incubated with the immunocomplex solution at room temperature for 30 minutes. Beads were then washed three times and processed for Western blotting.

Coomassie staining and mass-spectrometric analysis. After gel electrophoresis, staining was conducted for 30 min at room temperature using rapid Coomassie stain (Melford) diluted in 5% acetic acid, 7.5% methanol. To destain the gel, washings were afterward done with 5% acetic acid, 7.5% methanol solution, and repeated until the bands became visible. Relative to the protein ladder, the 230 kDa band of Nup358 was identified in the Nup358 immunoprecipitated sample, cut with a sterile scalpel and analyzed by mass spectrometry (Proteomic Unit, Cogentech).

RNA isolation and qRT-PCR. qRT-PCR was performed on 14 DIV, treated/untreated mouse cortical neurons obtained from three independent cultures. Total RNA was isolated with TRIZOL reagent (Thermo Fisher) and quantified using Nanodrop spectrophotometer. 1 µg of RNA was subjected to DNase I treatment and retro-transcribed using RevertAid First Strand cDNA Synthesis Kit (Thermo Fisher). The RT products were subjected to qPCR amplification of mouse *Nup358* and *GAPDH* using KAPA SYBR FAST qPCR Kit (KAPA Biosystems). These samples were incubated in the BioRad CFX96 Thermocycler according to the cycling conditions: 95°C for 3 min, followed by 40 cycles of 95°C for 10 s and 60°C for 30 s, and finally held at 4°C. The results obtained were analyzed with the Bio-Rad CFX Manager version 2.1 and the relative expression of mRNA was calculated based on the $2^{-\Delta\Delta Ct}$ method. The qRT-PCR was performed in technical duplicate and biological triplicate of independent cultures of 14 DIV mouse cortical neurons. For *Nup358* amplification, I used Mm.PT.58.9262525 PrimeTime qPCR primers, while for *GAPDH* amplification I used the primers: mGAPDH forward 5'- TTC ACC ACC ATG GAG AAG GC -3', and mGAPDH reverse 5'- GGC ATG GAC TGT GGT CAT GA -3'. All primers and probes used were purchased from IDT (TEMA Ricerca).

Statistical Analysis. All experiments were carried out in triplicates with independent mouse dissections. Immunofluorescent images are representative images of at least three independent experiments. Results are shown as means \pm SD, and evaluated by 2-tailed Student's t-test (two groups), or one-way ANOVA followed by Tukey's test (more than two groups) where $p < 0.05$ was considered statistically significant.

Bibliography

1. Mazzanti, M., Bustamante, J. O. & Oberleithner, H. Electrical dimension of the nuclear envelope. *Physiol. Rev.* **81**, 1–19 (2001).
2. Bastos, R., Panté, N. & Burke, B. Nuclear pore complex proteins. *Int. Rev. Cytol.* **162B**, 257–302 (1995).
3. D'Angelo, M. A. & Hetzer, M. W. The role of the nuclear envelope in cellular organization. *Cell. Mol. Life Sci.* **63**, 316–332 (2006).
4. Chatel, G. & Fahrenkrog, B. Dynamics and diverse functions of nuclear pore complex proteins. *Nucleus* **3**, 162–171 (2012).
5. Fawcett, D.W. (1981) *The Cell*. Second Edition. W. B. Saunders Co, Philadelphia, Pennsylvania. 303–368
6. Reichelt, R. *et al.* Correlation between structure and mass distribution of the nuclear pore complex and of distinct pore complex components. *J. Cell Biol.* **110**, 883–894 (1990).
7. Panté, N. & Aebi, U. Sequential binding of import ligands to distinct nucleopore regions during their nuclear import. *Science* **273**, 1729–1732 (1996).
8. Hurwitz, M. E. & Blobel, G. NUP82 is an essential yeast nucleoporin required for poly(A)⁺ RNA export. *J. Cell Biol.* **130**, 1275–1281 (1995).
9. Gall, J. G. Octagonal nuclear pores. *J. Cell Biol.* **32**, 391–399 (1967).
10. Beck, M., Lucić, V., Förster, F., Baumeister, W. & Medalia, O. Snapshots of nuclear pore complexes in action captured by cryo-electron tomography. *Nature* **449**, 611–615 (2007).
11. Stoffer, D. *et al.* Cryo-electron tomography provides novel insights into nuclear pore architecture: implications for nucleocytoplasmic transport. *J. Mol. Biol.* **328**, 119–130 (2003).
12. Lim, R. Y. H., Aebi, U. & Fahrenkrog, B. Towards reconciling structure and function in the nuclear pore complex. *Histochem. Cell Biol.* **129**, 105–116 (2008).
13. Maco, B., Fahrenkrog, B., Huang, N.-P. & Aebi, U. Nuclear pore complex structure and plasticity revealed by electron and atomic force microscopy. *Methods Mol. Biol.* **322**, 273–288 (2006).
14. Beck, M. *et al.* Nuclear pore complex structure and dynamics revealed by cryoelectron tomography. *Science* **306**, 1387–1390 (2004).
15. Beck, M. & Hurt, E. The nuclear pore complex: understanding its function through structural insight. *Nat. Rev. Mol. Cell Biol.* **18**, 73–89 (2017).
16. Franke, W. W. & Scheer, U. The ultrastructure of the nuclear envelope of amphibian oocytes: a reinvestigation. I. The mature oocyte. *J. Ultrastruct. Res.* **30**, 288–316 (1970).

17. Yang, Q., Rout, M. P. & Akey, C. W. Three-dimensional architecture of the isolated yeast nuclear pore complex: functional and evolutionary implications. *Mol. Cell* **1**, 223–234 (1998).
18. Suntharalingam, M. & Wente, S. R. Peering through the pore: nuclear pore complex structure, assembly, and function. *Dev. Cell* **4**, 775–789 (2003).
19. Jovanovic-Talisman, T. & Zilman, A. Protein transport by the nuclear pore complex: simple biophysics of a complex biomachine. *Biophys. J.* **113**, 6–14 (2017).
20. Adam, S. A. The nuclear pore complex. *Genome Biol.* **2**, REVIEWS0007 (2001).
21. Bruce Alberts, Alexander Johnson, Julian Lewis, David Morgan, Martin Raff, Keith Roberts, and Peter Walter. (2014). *Molecular Biology of The Cell*. Sixth Edition. Garland Science. Chapter 12: 651
22. Azimi, M. & Mofrad, M. R. K. Higher nucleoporin-Importin β affinity at the nuclear basket increases nucleocytoplasmic import. *PLoS ONE* **8**, e81741 (2013).
23. Cronshaw, J. M., Krutchinsky, A. N., Zhang, W., Chait, B. T. & Matunis, M. J. Proteomic analysis of the mammalian nuclear pore complex. *J. Cell Biol.* **158**, 915–927 (2002).
24. Alber, F. *et al.* The molecular architecture of the nuclear pore complex. *Nature* **450**, 695–701 (2007).
25. Schwartz, T. U. Modularity within the architecture of the nuclear pore complex. *Curr. Opin. Struct. Biol.* **15**, 221–226 (2005).
26. Devos, D. *et al.* Simple fold composition and modular architecture of the nuclear pore complex. *Proc Natl Acad Sci USA* **103**, 2172–2177 (2006).
27. Hoelz, A., Glavy, J. S. & Beck, M. Toward the atomic structure of the nuclear pore complex: when top down meets bottom up. *Nat. Struct. Mol. Biol.* **23**, 624–630 (2016).
28. Knockenhauer, K. E. & Schwartz, T. U. The nuclear pore complex as a flexible and dynamic gate. *Cell* **164**, 1162–1171 (2016).
29. Kelley, K., Knockenhauer, K. E., Kabachinski, G. & Schwartz, T. U. Atomic structure of the Y complex of the nuclear pore. *Nat. Struct. Mol. Biol.* **22**, 425–431 (2015).
30. Franz, C. *et al.* MEL-28/ELYS is required for the recruitment of nucleoporins to chromatin and postmitotic nuclear pore complex assembly. *EMBO Rep.* **8**, 165–172 (2007).
31. Liodice, I. The Entire Nup107-160 Complex, Including Three New Members, Is Targeted as One Entity to Kinetochores in Mitosis. *Molecular biology of the cell* **15**, 3333–3344 (2004).
32. Rasala, B. A., Orjalo, A. V., Shen, Z., Briggs, S. & Forbes, D. J. ELYS is a dual nucleoporin/kinetochore protein required for nuclear pore assembly and proper cell division. *Proc Natl Acad Sci USA* **103**, 17801–17806 (2006).

33. Siniosoglou, S. *et al.* A novel complex of nucleoporins, which includes Sec13p and a Sec13p homolog, is essential for normal nuclear pores. *Cell* **84**, 265–275 (1996).
34. Kampmann, M. & Blobel, G. Three-dimensional structure and flexibility of a membrane-coating module of the nuclear pore complex. *Nat. Struct. Mol. Biol.* **16**, 782–788 (2009).
35. Lutzmann, M., Kunze, R., Buerer, A., Aebi, U. & Hurt, E. Modular self-assembly of a Y-shaped multiprotein complex from seven nucleoporins. *EMBO J.* **21**, 387–397 (2002).
36. Bui, K. H. *et al.* Integrated structural analysis of the human nuclear pore complex scaffold. *Cell* **155**, 1233–1243 (2013).
37. Walther, T. C. *et al.* The conserved Nup107-160 complex is critical for nuclear pore complex assembly. *Cell* **113**, 195–206 (2003).
38. Harel, A. *et al.* Removal of a single pore subcomplex results in vertebrate nuclei devoid of nuclear pores. *Mol. Cell* **11**, 853–864 (2003).
39. von Appen, A. *et al.* In situ structural analysis of the human nuclear pore complex. *Nature* **526**, 140–143 (2015).
40. Eibauer, M. *et al.* Structure and gating of the nuclear pore complex. *Nat. Commun.* **6**, 7532 (2015).
41. Vollmer, B. & Antonin, W. The diverse roles of the Nup93/Nic96 complex proteins - structural scaffolds of the nuclear pore complex with additional cellular functions. *Biol. Chem.* **395**, 515–528 (2014).
42. Krull, S., Thyberg, J., Björkroth, B., Rackwitz, H.-R. & Cordes, V. C. Nucleoporins as components of the nuclear pore complex core structure and Tpr as the architectural element of the nuclear basket. *Mol. Biol. Cell* **15**, 4261–4277 (2004).
43. Grandi, P. *et al.* Nup93, a vertebrate homologue of yeast Nic96p, forms a complex with a novel 205-kDa protein and is required for correct nuclear pore assembly. *Mol. Biol. Cell* **8**, 2017–2038 (1997).
44. Dultz, E. *et al.* Systematic kinetic analysis of mitotic dis- and reassembly of the nuclear pore in living cells. *J. Cell Biol.* **180**, 857–865 (2008).
45. Finlay, D. R., Meier, E., Bradley, P., Horecka, J. & Forbes, D. J. A complex of nuclear pore proteins required for pore function. *J. Cell Biol.* **114**, 169–183 (1991).
46. Kita, K., Omata, S. & Horigome, T. Purification and characterization of a nuclear pore glycoprotein complex containing p62. *J. Biochem.* **113**, 377–382 (1993).
47. Buss, F. & Stewart, M. Macromolecular interactions in the nucleoporin p62 complex of rat nuclear pores: binding of nucleoporin p54 to the rod domain of p62. *J. Cell Biol.* **128**, 251–261 (1995).

48. Ulrich, A., Partridge, J. R. & Schwartz, T. U. The stoichiometry of the nucleoporin 62 subcomplex of the nuclear pore in solution. *Mol. Biol. Cell* **25**, 1484–1492 (2014).
49. Sachdev, R., Sieverding, C., Flötenmeyer, M. & Antonin, W. The C-terminal domain of Nup93 is essential for assembly of the structural backbone of nuclear pore complexes. *Mol. Biol. Cell* **23**, 740–749 (2012).
50. Chug, H., Trakhanov, S., Hülsmann, B. B., Pleiner, T. & Görlich, D. Crystal structure of the metazoan Nup62•Nup58•Nup54 nucleoporin complex. *Science* **350**, 106–110 (2015).
51. Allen, N. P., Huang, L., Burlingame, A. & Rexach, M. Proteomic analysis of nucleoporin interacting proteins. *J. Biol. Chem.* **276**, 29268–29274 (2001).
52. Terry, L. J. & Wente, S. R. Flexible gates: dynamic topologies and functions for FG nucleoporins in nucleocytoplasmic transport. *Eukaryotic Cell* **8**, 1814–1827 (2009).
53. Bestembayeva, A. *et al.* Nanoscale stiffness topography reveals structure and mechanics of the transport barrier in intact nuclear pore complexes. *Nat. Nanotechnol.* **10**, 60–64 (2015).
54. Labokha, A. A. *et al.* Systematic analysis of barrier-forming FG hydrogels from *Xenopus* nuclear pore complexes. *EMBO J.* **32**, 204–218 (2013).
55. Patel, S. S., Belmont, B. J., Sante, J. M. & Rexach, M. F. Natively unfolded nucleoporins gate protein diffusion across the nuclear pore complex. *Cell* **129**, 83–96 (2007).
56. Schmidt, H. B. & Görlich, D. Nup98 FG domains from diverse species spontaneously phase-separate into particles with nuclear pore-like permselectivity. *elife* **4**, (2015).
57. Eisenhardt, N., Redolfi, J. & Antonin, W. Interaction of Nup53 with Ndc1 and Nup155 is required for nuclear pore complex assembly. *J. Cell Sci.* **127**, 908–921 (2014).
58. Onischenko, E., Stanton, L. H., Madrid, A. S., Kieselbach, T. & Weis, K. Role of the Ndc1 interaction network in yeast nuclear pore complex assembly and maintenance. *J. Cell Biol.* **185**, 475–491 (2009).
59. Stavru, F. *et al.* NDC1: a crucial membrane-integral nucleoporin of metazoan nuclear pore complexes. *J. Cell Biol.* **173**, 509–519 (2006).
60. Jarnik, M. & Aebi, U. Toward a more complete 3-D structure of the nuclear pore complex. *J. Struct. Biol.* **107**, 291–308 (1991).
61. Goldberg, M. W. & Allen, T. D. High resolution scanning electron microscopy of the nuclear envelope: demonstration of a new, regular, fibrous lattice attached to the baskets of the nucleoplasmic face of the nuclear pores. *J. Cell Biol.* **119**, 1429–1440 (1992).

62. Frosst, P., Guan, T., Subauste, C., Hahn, K. & Gerace, L. Tpr is localized within the nuclear basket of the pore complex and has a role in nuclear protein export. *J. Cell Biol.* **156**, 617–630 (2002).
63. Cordes, V. C., Reidenbach, S., Rackwitz, H. R. & Franke, W. W. Identification of protein p270/Tpr as a constitutive component of the nuclear pore complex-attached intranuclear filaments. *J. Cell Biol.* **136**, 515–529 (1997).
64. Panté, N., Bastos, R., McMorro, I., Burke, B. & Aebi, U. Interactions and three-dimensional localization of a group of nuclear pore complex proteins. *J. Cell Biol.* **126**, 603–617 (1994).
65. Fornerod, M. *et al.* The human homologue of yeast CRM1 is in a dynamic subcomplex with CAN/Nup214 and a novel nuclear pore component Nup88. *EMBO J.* **16**, 807–816 (1997).
66. Walther, T. C. *et al.* The cytoplasmic filaments of the nuclear pore complex are dispensable for selective nuclear protein import. *J. Cell Biol.* **158**, 63–77 (2002).
67. Daigle, N. *et al.* Nuclear pore complexes form immobile networks and have a very low turnover in live mammalian cells. *J. Cell Biol.* **154**, 71–84 (2001).
68. D’Angelo, M. A., Raices, M., Panowski, S. H. & Hetzer, M. W. Age-dependent deterioration of nuclear pore complexes causes a loss of nuclear integrity in postmitotic cells. *Cell* **136**, 284–295 (2009).
69. Rabut, G., Doye, V. & Ellenberg, J. Mapping the dynamic organization of the nuclear pore complex inside single living cells. *Nat. Cell Biol.* **6**, 1114–1121 (2004).
70. Griffis, E. R., Altan, N., Lippincott-Schwartz, J. & Powers, M. A. Nup98 is a mobile nucleoporin with transcription-dependent dynamics. *Mol. Biol. Cell* **13**, 1282–1297 (2002).
71. Guan, T. *et al.* Nup50, a nucleoplasmically oriented nucleoporin with a role in nuclear protein export. *Mol. Cell. Biol.* **20**, 5619–5630 (2000).
72. Bodoor, K. *et al.* Sequential recruitment of NPC proteins to the nuclear periphery at the end of mitosis. *J. Cell Sci.* **112 (Pt 13)**, 2253–2264 (1999).
73. Enninga, J., Levay, A. & Fontoura, B. M. A. Sec13 shuttles between the nucleus and the cytoplasm and stably interacts with Nup96 at the nuclear pore complex. *Mol. Cell. Biol.* **23**, 7271–7284 (2003).
74. Nakielny, S., Shaikh, S., Burke, B. & Dreyfuss, G. Nup153 is an M9-containing mobile nucleoporin with a novel Ran-binding domain. *EMBO J.* **18**, 1982–1995 (1999).
75. Ball, J. R. & Ullman, K. S. Versatility at the nuclear pore complex: lessons learned from the nucleoporin Nup153. *Chromosoma* **114**, 319–330 (2005).
76. Griffis, E. R., Craige, B., Dimaano, C., Ullman, K. S. & Powers, M. A. Distinct functional domains within nucleoporins Nup153 and Nup98 mediate transcription-dependent mobility. *Mol. Biol. Cell* **15**, 1991–2002 (2004).

77. Nakano, H. *et al.* Unexpected role of nucleoporins in coordination of cell cycle progression. *Cell Cycle* **10**, 425–433 (2011).
78. Arib, G. & Akhtar, A. Multiple facets of nuclear periphery in gene expression control. *Curr. Opin. Cell Biol.* **23**, 346–353 (2011).
79. Capelson, M., Doucet, C. & Hetzer, M. W. Nuclear pore complexes: guardians of the nuclear genome. *Cold Spring Harb. Symp. Quant. Biol.* **75**, 585–597 (2010).
80. Delphin, C., Guan, T., Melchior, F. & Gerace, L. RanGTP targets p97 to RanBP2, a filamentous protein localized at the cytoplasmic periphery of the nuclear pore complex. *Mol. Biol. Cell* **8**, 2379–2390 (1997).
81. Bernad, R., van der Velde, H., Fornerod, M. & Pickersgill, H. Nup358/RanBP2 attaches to the nuclear pore complex via association with Nup88 and Nup214/CAN and plays a supporting role in CRM1-mediated nuclear protein export. *Mol. Cell. Biol.* **24**, 2373–2384 (2004).
82. Yokoyama, N. *et al.* A giant nucleopore protein that binds Ran/TC4. *Nature* **376**, 184–188 (1995).
83. Wu, J., Matunis, M. J., Kraemer, D., Blobel, G. & Coutavas, E. Nup358, a cytoplasmically exposed nucleoporin with peptide repeats, Ran-GTP binding sites, zinc fingers, a cyclophilin A homologous domain, and a leucine-rich region. *J. Biol. Chem.* **270**, 14209–14213 (1995).
84. Chook, Y. M. & Blobel, G. Karyopherins and nuclear import. *Curr. Opin. Struct. Biol.* **11**, 703–715 (2001).
85. Cook, A., Bono, F., Jinek, M. & Conti, E. Structural biology of nucleocytoplasmic transport. *Annu. Rev. Biochem.* **76**, 647–671 (2007).
86. Vetter, I. R., Nowak, C., Nishimoto, T., Kuhlmann, J. & Wittinghofer, A. Structure of a Ran-binding domain complexed with Ran bound to a GTP analogue: implications for nuclear transport. *Nature* **398**, 39–46 (1999).
87. Reverter, D. & Lima, C. D. Insights into E3 ligase activity revealed by a SUMO-RanGAP1-Ubc9-Nup358 complex. *Nature* **435**, 687–692 (2005).
88. Geyer, J. P. *et al.* Solution structure of the Ran-binding domain 2 of RanBP2 and its interaction with the C terminus of Ran. *J. Mol. Biol.* **348**, 711–725 (2005).
89. Kassube, S. A. *et al.* Crystal structure of the N-terminal domain of Nup358/RanBP2. *J. Mol. Biol.* **423**, 752–765 (2012).
90. Lin, D. H., Zimmermann, S., Stuwe, T., Stuwe, E. & Hoelz, A. Structural and functional analysis of the C-terminal domain of Nup358/RanBP2. *J. Mol. Biol.* **425**, 1318–1329 (2013).
91. Görlich, D. & Mattaj, I. W. Nucleocytoplasmic transport. *Science* **271**, 1513–1518 (1996).
92. Wenthe, S. R. & Rout, M. P. The nuclear pore complex and nuclear transport. *Cold Spring Harb. Perspect. Biol.* **2**, a000562 (2010).

93. Hamada, M. *et al.* Ran-dependent docking of importin-beta to RanBP2/Nup358 filaments is essential for protein import and cell viability. *J. Cell Biol.* **194**, 597–612 (2011).
94. Terry, L. J., Shows, E. B. & Wente, S. R. Crossing the nuclear envelope: hierarchical regulation of nucleocytoplasmic transport. *Science* **318**, 1412–1416 (2007).
95. Monecke, T. *et al.* Crystal structure of the nuclear export receptor CRM1 in complex with Snurportin1 and RanGTP. *Science* **324**, 1087–1091 (2009).
96. Matunis, M. J., Wu, J. & Blobel, G. SUMO-1 modification and its role in targeting the Ran GTPase-activating protein, RanGAP1, to the nuclear pore complex. *J. Cell Biol.* **140**, 499–509 (1998).
97. Ritterhoff, T. *et al.* The RanBP2/RanGAP1*SUMO1/Ubc9 SUMO E3 ligase is a disassembly machine for Crm1-dependent nuclear export complexes. *Nat. Commun.* **7**, 11482 (2016).
98. Singh, B. B., Patel, H. H., Roepman, R., Schick, D. & Ferreira, P. A. The zinc finger cluster domain of RanBP2 is a specific docking site for the nuclear export factor, exportin-1. *J. Biol. Chem.* **274**, 37370–37378 (1999).
99. Forler, D. *et al.* RanBP2/Nup358 provides a major binding site for NXF1-p15 dimers at the nuclear pore complex and functions in nuclear mRNA export. *Mol. Cell. Biol.* **24**, 1155–1167 (2004).
100. Kuersten, S., Ohno, M. & Mattaj, I. W. Nucleocytoplasmic transport: Ran, beta and beyond. *Trends Cell Biol.* **11**, 497–503 (2001).
101. Neilson, D. E. *et al.* Infection-triggered familial or recurrent cases of acute necrotizing encephalopathy caused by mutations in a component of the nuclear pore, RANBP2. *Am. J. Hum. Genet.* **84**, 44–51 (2009).
102. Aslanukov, A. *et al.* RanBP2 modulates Cox11 and hexokinase I activities and haploinsufficiency of RanBP2 causes deficits in glucose metabolism. *PLoS Genet.* **2**, e177 (2006).
103. Cho, K.-I. *et al.* Loss of Ranbp2 in motoneurons causes disruption of nucleocytoplasmic and chemokine signaling, proteostasis of hnRNPH3 and Mmp28, and development of amyotrophic lateral sclerosis-like syndromes. *Dis. Model. Mech.* **10**, 559–579 (2017).
104. Um, J. W. *et al.* Parkin ubiquitinates and promotes the degradation of RanBP2. *J. Biol. Chem.* **281**, 3595–3603 (2006).
105. Patil, H. *et al.* Impairments in age-dependent ubiquitin proteostasis and structural integrity of selective neurons by uncoupling Ran GTPase from the Ran-binding domain 3 of Ranbp2 and identification of novel mitochondrial isoforms of ubiquitin-conjugating enzyme E2I (ubc9) and Ranbp2. *Small GTPases* 1–16 (2017). doi:10.1080/21541248.2017.1356432

106. Güttinger, S., Laurell, E. & Kutay, U. Orchestrating nuclear envelope disassembly and reassembly during mitosis. *Nat. Rev. Mol. Cell Biol.* **10**, 178–191 (2009).
107. Joseph, J., Liu, S.-T., Jablonski, S. A., Yen, T. J. & Dasso, M. The RanGAP1-RanBP2 complex is essential for microtubule-kinetochore interactions in vivo. *Curr. Biol.* **14**, 611–617 (2004).
108. Salina, D., Enarson, P., Rattner, J. B. & Burke, B. Nup358 integrates nuclear envelope breakdown with kinetochore assembly. *J. Cell Biol.* **162**, 991–1001 (2003).
109. Dawlaty, M. M. *et al.* Resolution of sister centromeres requires RanBP2-mediated SUMOylation of topoisomerase IIalpha. *Cell* **133**, 103–115 (2008).
110. Hashizume, C., Kobayashi, A. & Wong, R. W. Down-modulation of nucleoporin RanBP2/Nup358 impaired chromosomal alignment and induced mitotic catastrophe. *Cell Death Dis.* **4**, e854 (2013).
111. Joseph, J. & Dasso, M. The nucleoporin Nup358 associates with and regulates interphase microtubules. *FEBS Lett.* **582**, 190–196 (2008).
112. Mahadevan, K. *et al.* RanBP2/Nup358 potentiates the translation of a subset of mRNAs encoding secretory proteins. *PLoS Biol.* **11**, e1001545 (2013).
113. Sahoo, M. R. *et al.* Nup358 binds to AGO proteins through its SUMO-interacting motifs and promotes the association of target mRNA with miRISC. *EMBO Rep.* **18**, 241–263 (2017).
114. Fauser, S., Aslanukov, A., Roepman, R. & Ferreira, P. A. Genomic organization, expression, and localization of murine Ran-binding protein 2 (RanBP2) gene. *Mamm. Genome* **12**, 406–415 (2001).
115. Mavlyutov, T. A., Cai, Y. & Ferreira, P. A. Identification of RanBP2- and kinesin-mediated transport pathways with restricted neuronal and subcellular localization. *Traffic* **3**, 630–640 (2002).
116. Ferreira, P. A., Nakayama, T. A., Pak, W. L. & Travis, G. H. Cyclophilin-related protein RanBP2 acts as chaperone for red/green opsin. *Nature* **383**, 637–640 (1996).
117. Ferreira, P. A., Nakayama, T. A. & Travis, G. H. Interconversion of red opsin isoforms by the cyclophilin-related chaperone protein Ran-binding protein 2. *Proc Natl Acad Sci USA* **94**, 1556–1561 (1997).
118. Cai, Y., Singh, B. B., Aslanukov, A., Zhao, H. & Ferreira, P. A. The docking of kinesins, KIF5B and KIF5C, to Ran-binding protein 2 (RanBP2) is mediated via a novel RanBP2 domain. *J. Biol. Chem.* **276**, 41594–41602 (2001).
119. Cho, K. *et al.* Association of the kinesin-binding domain of RanBP2 to KIF5B and KIF5C determines mitochondria localization and function. *Traffic* **8**, 1722–1735 (2007).

120. Ferreira, P. A., Yunfei, C., Schick, D. & Roepman, R. The cyclophilin-like domain mediates the association of Ran-binding protein 2 with subunits of the 19 S regulatory complex of the proteasome. *J. Biol. Chem.* **273**, 24676–24682 (1998).
121. Vyas, P., Singh, A., Murawala, P. & Joseph, J. Nup358 interacts with Dishevelled and aPKC to regulate neuronal polarity. *Biol. Open* **2**, 1270–1278 (2013).
122. Dotti, C. G., Sullivan, C. A. & Banker, G. A. The establishment of polarity by hippocampal neurons in culture. *J. Neurosci.* **8**, 1454–1468 (1988).
123. Sakakibara, A. & Hatanaka, Y. Neuronal polarization in the developing cerebral cortex. *Front. Neurosci.* **9**, 116 (2015).
124. Arimura, N. & Kaibuchi, K. Neuronal polarity: from extracellular signals to intracellular mechanisms. *Nat. Rev. Neurosci.* **8**, 194–205 (2007).
125. Yoshimura, T. & Rasband, M. N. Axon initial segments: diverse and dynamic neuronal compartments. *Curr. Opin. Neurobiol.* **27**, 96–102 (2014).
126. Song, A.-H. *et al.* A selective filter for cytoplasmic transport at the axon initial segment. *Cell* **136**, 1148–1160 (2009).
127. Grubb, M. S. & Burrone, J. Building and maintaining the axon initial segment. *Curr. Opin. Neurobiol.* **20**, 481–488 (2010).
128. Rasband, M. N. The axon initial segment and the maintenance of neuronal polarity. *Nat. Rev. Neurosci.* **11**, 552–562 (2010).
129. Kole, M. H. P. & Stuart, G. J. Signal processing in the axon initial segment. *Neuron* **73**, 235–247 (2012).
130. Leterrier, C. The axon initial segment: an updated viewpoint. *J. Neurosci.* **38**, 2135–2145 (2018).
131. Grubb, M. S. & Burrone, J. Activity-dependent relocation of the axon initial segment fine-tunes neuronal excitability. *Nature* **465**, 1070–1074 (2010).
132. Kuba, H., Oichi, Y. & Ohmori, H. Presynaptic activity regulates Na(+) channel distribution at the axon initial segment. *Nature* **465**, 1075–1078 (2010).
133. Coles, C. H. & Bradke, F. Coordinating neuronal actin-microtubule dynamics. *Curr. Biol.* **25**, R677-91 (2015).
134. Pan, Z. *et al.* A common ankyrin-G-based mechanism retains KCNQ and NaV channels at electrically active domains of the axon. *J. Neurosci.* **26**, 2599–2613 (2006).
135. Rasmussen, H. B. *et al.* Requirement of subunit co-assembly and ankyrin-G for M-channel localization at the axon initial segment. *J. Cell Sci.* **120**, 953–963 (2007).
136. Hedstrom, K. L., Ogawa, Y. & Rasband, M. N. AnkyrinG is required for maintenance of the axon initial segment and neuronal polarity. *J. Cell Biol.* **183**, 635–640 (2008).
137. Benvegnù, S., Mateo, M. I., Palomer, E., Jurado-Arjona, J. & Dotti, C. G. Aging triggers cytoplasmic depletion and nuclear translocation of the E3 ligase

- mahogunin: a function for ubiquitin in neuronal survival. *Mol. Cell* **66**, 358–372.e7 (2017).
138. La Montanara, P. *et al.* Synaptic synthesis, dephosphorylation, and degradation: a novel paradigm for an activity-dependent neuronal control of CDKL5. *J. Biol. Chem.* **290**, 4512–4527 (2015).
 139. Schor, I. E., Rascovan, N., Pelisch, F., Alló, M. & Kornblihtt, A. R. Neuronal cell depolarization induces intragenic chromatin modifications affecting NCAM alternative splicing. *Proc Natl Acad Sci USA* **106**, 4325–4330 (2009).
 140. Wayman, G. A. *et al.* Activity-dependent dendritic arborization mediated by CaM-kinase I activation and enhanced CREB-dependent transcription of Wnt-2. *Neuron* **50**, 897–909 (2006).
 141. Redmond, L., Kashani, A. H. & Ghosh, A. Calcium regulation of dendritic growth via CaM kinase IV and CREB-mediated transcription. *Neuron* **34**, 999–1010 (2002).
 142. Saneyoshi, T. *et al.* Activity-dependent synaptogenesis: regulation by a CaM-kinase kinase/CaM-kinase I/betaPIX signaling complex. *Neuron* **57**, 94–107 (2008).
 143. Zhang, P. & Lisman, J. E. Activity-dependent regulation of synaptic strength by PSD-95 in CA1 neurons. *J. Neurophysiol.* **107**, 1058–1066 (2012).
 144. Winckler, B., Forscher, P. & Mellman, I. A diffusion barrier maintains distribution of membrane proteins in polarized neurons. *Nature* **397**, 698–701 (1999).
 145. Sánchez-Ponce, D., DeFelipe, J., Garrido, J. J. & Muñoz, A. Developmental expression of Kv potassium channels at the axon initial segment of cultured hippocampal neurons. *PLoS ONE* **7**, e48557 (2012).
 146. Leterrier, C. & Dargent, B. No Pasaran! Role of the axon initial segment in the regulation of protein transport and the maintenance of axonal identity. *Semin. Cell Dev. Biol.* **27**, 44–51 (2014).
 147. Jones, S. L. & Svitkina, T. M. Axon initial segment cytoskeleton: architecture, development, and role in neuron polarity. *Neural Plast.* **2016**, 6808293 (2016).
 148. Zhou, D. *et al.* AnkyrinG is required for clustering of voltage-gated Na channels at axon initial segments and for normal action potential firing. *J. Cell Biol.* **143**, 1295–1304 (1998).
 149. Hedstrom, K. L. *et al.* Neurofascin assembles a specialized extracellular matrix at the axon initial segment. *J. Cell Biol.* **178**, 875–886 (2007).
 150. Agostini, M. *et al.* Metabolic reprogramming during neuronal differentiation. *Cell Death Differ.* **23**, 1502–1514 (2016).
 151. Li, Z., Okamoto, K.-I., Hayashi, Y. & Sheng, M. The importance of dendritic mitochondria in the morphogenesis and plasticity of spines and synapses. *Cell* **119**, 873–887 (2004).

152. Raghunayakula, S., Subramonian, D., Dasso, M., Kumar, R. & Zhang, X.-D. Molecular characterization and functional analysis of annulate lamellae pore complexes in nuclear transport in mammalian cells. *PLoS ONE* **10**, e0144508 (2015).
153. Kole, M. H. P., Letzkus, J. J. & Stuart, G. J. Axon initial segment Kv1 channels control axonal action potential waveform and synaptic efficacy. *Neuron* **55**, 633–647 (2007).
154. Kole, M. H. P. *et al.* Action potential generation requires a high sodium channel density in the axon initial segment. *Nat. Neurosci.* **11**, 178–186 (2008).
155. Leterrier, C. *et al.* Ankyrin G membrane partners drive the establishment and maintenance of the axon initial segment. *Front. Cell. Neurosci.* **11**, 6 (2017).
156. Boiko, T. *et al.* Ankyrin-dependent and -independent mechanisms orchestrate axonal compartmentalization of L1 family members neurofascin and L1/neuron-glia cell adhesion molecule. *J. Neurosci.* **27**, 590–603 (2007).
157. He, M., Jenkins, P. & Bennett, V. Cysteine 70 of ankyrin-G is S-palmitoylated and is required for function of ankyrin-G in membrane domain assembly. *J. Biol. Chem.* **287**, 43995–44005 (2012).
158. Fujiwara, Y. *et al.* Structural basis for the membrane association of ankyrinG via palmitoylation. *Sci. Rep.* **6**, 23981 (2016).
159. Qian, X., Goderie, S. K., Shen, Q., Stern, J. H. & Temple, S. Intrinsic programs of patterned cell lineages in isolated vertebrate CNS ventricular zone cells. *Development* **125**, 3143–3152 (1998).
160. Goetze, B. *et al.* The brain-specific double-stranded RNA-binding protein Staufen2 is required for dendritic spine morphogenesis. *J. Cell Biol.* **172**, 221–231 (2006).
161. Goetze, B., Grunewald, B., Baldassa, S. & Kiebler, M. Chemically controlled formation of a DNA/calcium phosphate coprecipitate: application for transfection of mature hippocampal neurons. *J. Neurobiol.* **60**, 517–525 (2004).